Theoretical Investigation of the Triggering of Neoclassical Tearing Modes by Transient Resonant Magnetic Perturbations in NSTX

R. Fitzpatrick [a]

Institute for Fusion Studies, Department of Physics,

University of Texas at Austin, Austin TX 78712, USA.

[a] rfitzp@utexas.edu

I. INTRODUCTION

Neoclassical tearing modes (NTMs) are the main obstacle to obtaining normalized plasma pressure (β) levels in tokamak[1] plasmas that are adequate for achieving thermonuclear fusion.[2,3] NTMs were originally identified experimentally on the TFTR tokamak.[4] NTMs lead to the generation of low poloidal and toroidal mode number (m and n) magnetic island chains on toroidal magnetic flux-surfaces within the plasma that are characterized by rational (i.e., m/n) values of the safety-factor (q). An NTM is driven by a helical hole in the bootstrap current[5] profile that arises as a consequence of the flattening of the plasma pressure across the associated island chain region.[6] However, a magnetic island chain can only locally flatten the plasma pressure when its radial width exceeds a certain threshold value that depends on the local ratio of the parallel and perpendicular energy diffusivities.[7] This leads to the conclusion that NTMs are actually meta-stable. In other words, some sort of seed perturbation must be applied to the relevant rational magnetic flux-surface in order to trigger an NTM. In practice, the seed perturbation usually takes the form of a transient magnetic perturbation that is resonant at the rational surface. Such perturbations are generated in tokamak plasmas primarily by sawtooth crashes, edge localized modes, and fishbones.[2,3]

The aim of this paper is to investigate how the properties (i.e., amplitude, duration, and rotation frequency) of a transient resonant magnetic perturbation (RMP) applied to a toroidal tokamak plasma affect its ability to trigger NTMs within the plasma. In this study, we shall use the EPEC code (see Sect. II) to simulate what happens when a transient $n = 1$ magnetic perturbation is applied to a typical NSTX plasma.

II. BRIEF DESCRIPTION OF EPEC CODE

The EPEC code[8–11] employs an asymptotic matching[12–22] approach to determine the resistive response of a toroidal tokamak equilibrium to an applied RMP. The main advantage of the asymptotic matching approach is that it largely removes the very short Alfvén time from the problem. In fact, the EPEC code is capable of accurately simulating the resistive response of a toroidal tokamak plasma to an RMP while taking time steps that extend over many Alfvén times. In this manner, the code is able to simulate a complete plasma discharge

in a matter of minutes of real time.

The version of the EPEC model used in this paper is described in detail in Appendix A. The EPEC model is fully toroidal, and makes use of experimental magnetic equilibrium data (gfiles) and plasma profile data (pfiles). The model incorporates an accurate neoclassical model [23] that takes impurities and neutral particles into account, and allows the calculation of the neoclassical poloidal flow-damping timescale, the charge-exchange damping timescale, the neoclassical ion rotation profile, and the bootstrap current profile. The model also includes perturbed bootstrap current, magnetic field-line curvature, ion polarization current, and island saturation terms in the resonant plasma response model that governs the growth of magnetic island chains at the various rational surfaces within the plasma. Finally, the model accurately calculates the critical island widths needed to locally flatten the plasma pressure profile.

III. NSTX DISCHARGE 127317

A. Introduction

The two NSTX discharges studied in this paper were chosen because they were both fairly generic and had precomputed kinetic-EFITs.

The first discharge studied in this paper is 127317, which was one of the discharges used in an investigation of the interaction between edge localized modes (ELMs) and RMPs in NSTX.[24] Discharge 127317 is an H-mode discharge, characterized by a double magnetic null boundary shape, 6 MW of neutral beam heating power, and no lithium coating of the walls.

B. Magnetic Equilibrium

Figure 1 shows the magnetic equilibrium of NSTX discharge 127317 at $t = 400$ ms. This equilibrium is characterized by a scale major radius $R_0 = 0.85$ m (see Sect. A 2 a), a scale toroidal magnetic field-strength $B_0 = 0.44$ T (see Sect. A 2 b), a net toroidal plasma current $I_\phi = 753$ kA, a safety-factor at the 95% flux-surface $q_{95} = 11.0$, and a poloidal beta $\beta_p = 0.61$.

C. Plasma Profiles

Figure 2 shows the safety-factor, electron number density, electron temperature, impurity ion number density, and impurity ion toroidal angular velocity profiles in NSTX discharge 127317 at $t = 400$ ms. The majority ions are deuterium, and the impurities are assumed to be fully-stripped carbon ions. Note that the discharge is subject to rotation braking due to an applied $n = 3$ RMP, which accounts for the lower than usual toroidal rotation. Because there is no poloidal impurity ion rotation data for this discharge, the $\mathbf{E} \times \mathbf{B}$ rotation profile is deduced from the toroidal impurity ion rotation data using neoclassical theory. (See Sect. A 3 g.)

The perpendicular electron energy diffusivity (χ_e), perpendicular ion energy diffusivity (χ_i), perpendicular toroidal momentum diffusivity (χ_ϕ), and perpendicular particle diffusivity ($D_\perp$) are given the plausible values 1.0, 1.0, 1.0, and 0.2 m^2/s, respectively, throughout the plasma.

The flux-surface averaged neutral deuterium atom number density takes the form $\langle n_n \rangle(r) = \langle n_n \rangle(r_{100})/[1 + (r - r_{100})^2/l_n^2]$, where $\langle n_n \rangle(r_{100}) = 1.0 \times 10^{16}\,\mathrm{m}^{-3}$, and $l_n = 1.3 \times 10^{-2}\,\mathrm{m}$. The flux-surface neutral poloidal asymmetry parameter is given the value $y_n = 1.5$. (See Sect. A 3 e.) The flux-surface averaged deuterium-atom/deuterium-ion charge-exchange rate constant is $\langle \sigma\, v \rangle_i^{\mathrm{cx}} = 4 \times 10^{-14}\,\mathrm{m}^3\,\mathrm{s}^{-1}$.[25] The neutrals are assumed to be hot (i.e., $E_n/T_i = 1$.) Note that neutrals do not really play a role in the physics of NTMs, which are resonant in the plasma core, and are only included in the calculation because they need to be specified in the EPEC model.

D. NTM Stability

IV. NSTX DISCHARGE 139057

A. Introduction

The second discharge studied in this paper is 139057, which was one of the discharges used in an investigation of blob dynamics in NSTX.[26] Discharge 139057 is an H-mode discharge, characterized by a single magnetic null boundary shape, 6 MW of neutral beam heating power, and lithium coating of the walls.

B. Magnetic Equilibrium

Figure 11 shows the magnetic equilibrium of NSTX discharge 139057 at $t = 557$ ms. This equilibrium is characterized by a scale major radius $R_0 = 0.85$ m, a scale toroidal magnetic field-strength $B_0 = 0.54$ T, a net toroidal plasma current $I_\phi = 907$ kA, a safety-factor at the 95% flux-surface $q_{95} = 9.5$, and a poloidal beta $\beta_p = 0.57$.

C. Plasma Profiles

Figure 12 shows the safety-factor, electron number density, electron temperature, impurity ion number density, and impurity ion toroidal angular velocity profiles in NSTX discharge 139057 at $t = 557$ ms. As before, the majority ions are deuterium, and the impurities are assumed to be fully-stripped carbon ions. Note that the discharge is not subject to rotation braking due to an applied $n = 3$ RMP, which accounts for the higher toroidal rotation than that in discharge 127317. As before, the $\mathbf{E} \times \mathbf{B}$ rotation profile is deduced from the toroidal impurity ion rotation data using neoclassical theory.

The diffusivity and neutral profiles in discharge 139057 are assumed to be the same as those adopted in the study of discharge 127317.

D. NTM Stability

V. SUMMARY AND CONCLUSIONS

ACKNOWLEDGEMENTS

The author would also like to thank J.-K. Park and N.C. Logan for their advice on how to run the GPEC code. Part of the data analysis was performed using the OMFIT integrated modeling framework.[27]

This research was directly funded by the U.S. Department of Energy, Office of Science, Office of Fusion Energy Sciences, under contract DE-SC0021156.

Appendix A: Description of EPEC Model

1. Introduction

The (Extended Perturbed Equilibrium Code) EPEC model was introduced in Ref. 8, and imporved in Refs. 9, 10, and 11. The model has been further extended for the study presented in this paper. The latest improvements to the model include the introduction of perturbed bootstrap current, magnetic field-line curvature, ion polarization current, and island saturation terms into the resonant plasma response model (see Sects. A 2 e, A 3 e, A 3 f, and A 4 d), a more accurate calculation of the critical island widths needed to locally flatten the electron temperature, the ion temperature, and the electron number density profiles (see Sect. A 4 c), and a better calculation of the natural frequencies of tearing modes (see Sect. A 5 b).

2. Plasma Response in Outer Region

a. Coordinates

Let R, ϕ, and Z be right-handed cylindrical coordinates whose symmetry axis corresponds to the toroidal symmetry axis of the plasma. Let r, θ, and ϕ be right-handed flux coordinates whose Jacobian is $\mathcal{J} \equiv (\nabla r \times \nabla\theta \cdot \nabla\phi)^{-1} = r\,R^2/R_0$. Here, R_0 is a convenient scale major radius, r is a magnetic flux-surface label with dimensions of length, and θ is an axisymmetric angular coordinate that increases by 2π radians for every poloidal circuit of the magnetic axis. Let $r = 0$ correspond to the magnetic axis, and let $r = r_{100}$ correspond to the last closed magnetic flux-surface.

b. Equilibrium Magnetic Field

The equilibrium magnetic field is written $\mathbf{B} = R_0\,B_0\,[f(r)\,\nabla\phi \times \nabla r + g(r)\,\nabla\phi]$, where B_0 is a convenient scale toroidal magnetic field-strength, and $q(r) = r\,g/(R_0\,f)$ is the safety-factor profile.[8] The equilibrium poloidal magnetic flux, $\Psi_p(r)$, satisfies $d\Psi_p/dr = R_0\,B_0\,f(r)$, where, by convention, $\Psi_p(r_{100}) = 0$. The normalized poloidal magnetic flux, $\Psi_N(r)$, is defined such that $\Psi_N(r) = 1 - \Psi_p(r)/\Psi_p(0)$. Hence, $\Psi_N(0) = 0$ and $\Psi_N(r_{100}) = 1$.

c. Perturbed Magnetic Field

Consider the response of the plasma to an RMP with $n > 0$ periods in the toroidal direction. We can write the components of the perturbed magnetic field in the form [8]

$$\frac{r\,R^2\,\delta\mathbf{B}\cdot\nabla r}{R_0^2} = \mathrm{i}\sum_j \psi_j(r)\,\mathrm{e}^{\,\mathrm{i}\,(m_j\theta - n\,\phi)}, \tag{A1}$$

$$R^2\,\delta\mathbf{B}\cdot\nabla\phi = n\sum_j \frac{\Xi_j(r)}{m_j}\,\mathrm{e}^{\,\mathrm{i}\,(m_j\,\theta - n\,\phi)}, \tag{A2}$$

where the sum is over all relevant poloidal harmonics of the perturbed magnetic field.

Let there be K resonant (i.e., rational) magnetic flux-surfaces in the plasma, labelled 1 through K. Consider the kth resonant surface, $r = r_k$, at which $q(r_k) = m_k/n$, where m_k is a positive integer. Let $\Psi_k = \psi_k(r_k)/m_k$, and $\Delta\Psi_k = [\Xi_k]_{r_{k-}}^{r_{k+}}$. Here, Ψ_k is the (complex) reconnected helical magnetic flux at the kth resonant surface, whereas $\Delta\Psi_k$ is a (complex) measure of the strength of the current sheet at the same resonant surface.

d. Toroidal Tearing Mode Dispersion Relation

In the presence of the RMP, the Ψ_k and the $\Delta\Psi_k$ values are related according to the inhomogeneous toroidal tearing mode dispersion relation, which takes the form [8,18]

$$\Delta\Psi_k = \sum_{k'=1,K} E_{kk'}\,\Psi_{k'} + |E_{kk}|\,\chi_k. \tag{A3}$$

Here, $E_{kk'}$ (for k, $k' = 1$, K) is the dimensionless, Hermitian, toroidal tearing mode stability matrix,[18] whereas the χ_k (for $k = 1, K$) parameterize the current sheets driven at the various resonant surfaces when the plasma responds to the applied RMP in accordance with the equations of linearized, marginally-stable, ideal-MHD.

The EPEC model determines the elements of the $E_{kk'}$ matrix using a high-q approximation. In fact, if $F_{kk'}$ is the inverse of the $E_{kk'}$ matrix then [8]

$$F_{kk'} = \oint\oint G(R_k, Z_k; R_{k'}, Z_{k'})\,\mathrm{e}^{-\mathrm{i}\,(m_k\,\theta_k - m_{k'}\,\theta_{k'})}\,\frac{d\theta_k}{2\pi}\,\frac{d\theta_{k'}}{2\pi}, \tag{A4}$$

and

$$G(R_k, Z_k; R_{k'}, Z_{k'}) = \frac{(-1)^{\,n}\,\pi^{\,2}\,R_k\,R_{k'}/R_0}{2\,\Gamma(1/2)\,\Gamma(n+1/2)}\left[\frac{\cosh\eta_{kk'}}{R_k^2 + R_{k'}^2 + (Z_k - Z_{k'})^{\,2}}\right]^{1/2}$$

$$\times \left[(n-1/2)\, P^{n-1}_{-1/2}(\cosh\eta_{kk'}) + \frac{P^{n+1}_{-1/2}(\cosh\eta_{kk'})}{n+1/2} \right], \tag{A5}$$

with

$$\eta_{kk'} = \tanh^{-1}\left[\frac{2\, R_k\, R_{k'}}{R_k^2 + R_{k'}^2 + (Z_k - Z_{k'})^2} \right]. \tag{A6}$$

Here, the double integral in Eq. (A4) is taken around the kth resonant surface and the k'th resonant surface. Finally, the $\Gamma(z)$ and $P^{\nu}_{\mu}(z)$ are gamma functions and associated Legendre functions, respectively.

The (complex) χ_k parameters are determined from the GPEC code.[28] To be more exact, the GPEC code calculates the (complex) dimensionless $\Delta_{m_k\, n}$ parameters which measure the strengths of the ideal current sheets that develop at the various resonant magnetic flux-surfaces in the plasma in response to the applied RMP. The $\Delta_{m_k\, n}$ parameters are related to the χ_k parameters according to

$$\frac{\chi_k}{R_0\, B_0} = -\mathrm{i}\, \frac{\Delta_{m_k\, n}}{|E_{kk}|} \left(\frac{r_k}{R_0} \right)^2 \frac{g(r_k)}{m_k\, [a_{kk}(r_k) + (r_k/R_0\, q_k)^2]}, \tag{A7}$$

where $q_k = m_k/n$, and $a_{kk}(r) = \oint |\nabla r|^{-2}\, d\theta/(2\pi)$.

e. Glasser-Greene-Johnson Parameters

Let us write $\mathbf{B} = \nabla\phi\times\nabla\psi_p + g(\psi_p)\,\nabla\phi$. The angle θ^* is defined such that $\nabla\phi\times\nabla\psi_p\cdot\nabla\theta^* = \gamma(\psi_p)\, B$. Let

$$J_1(\psi_p) = \oint \frac{1}{B}\, \frac{d\theta^*}{2\pi}, \tag{A8}$$

$$J_2(\psi_p) = \oint B\, \frac{d\theta^*}{2\pi}, \tag{A9}$$

$$J_3(\psi_p) = \oint \frac{1}{B^3}\, \frac{d\theta^*}{2\pi}, \tag{A10}$$

$$J_4(\psi_p) = \oint \frac{1}{B\, |\nabla\psi_p|^2}\, \frac{d\theta^*}{2\pi}, \tag{A11}$$

$$J_5(\psi_p) = \oint \frac{B}{|\nabla\psi_p|^2}\, \frac{d\theta^*}{2\pi}, \tag{A12}$$

$$J_6(\psi_p) = \oint \frac{1}{B^3\, |\nabla\psi_p|^2}\, \frac{d\theta^*}{2\pi}. \tag{A13}$$

It follows that [29]

$$E(\psi_p) = -\frac{dP/d\psi_p}{(dq/d\psi_p)^2}\, \frac{1}{\gamma} \left[\frac{d}{d\psi_p}\left(\frac{J_1}{\gamma} \right) - g\, \frac{dq}{d\psi_p}\, \frac{J_1}{J_2} \right] J_5, \tag{A14}$$

$$F(\psi_p) = \frac{(dP/d\psi_p)^2}{(dq/d\psi_p)^2}\,\frac{1}{\gamma^2}\left[g^2\left(J_5\,J_6 - J_4^2\right) + J_5\,J_3\right], \tag{A15}$$

$$H(\psi_p) = \frac{dP/d\psi_p}{dq/d\psi_p}\,\frac{g}{\gamma}\left(J_4 - \frac{J_1\,J_5}{J_2}\right), \tag{A16}$$

where $P(\psi_p)$ is the total plasma pressure. Finally, $D_R(\psi_p) = E + F + H^2$.

f. Current Gradient Parameters

The normalized toroidal plasma current density profile is written

$$\hat{J}_\phi(r) = -\frac{\mu_0\,R_0\,R}{B_0}\,\frac{dP}{d\Psi_p} - R_0^2\,B_0\,g\,\frac{dg}{d\Psi_p}. \tag{A17}$$

The previous expression is evaluated on the outboard mid-plane. Let $\hat{J}'_\phi = d\hat{J}_\phi/dr$, $\hat{J}''_\phi = d^2\hat{J}_\phi/dr^2$, $s(r) = d\ln q/d\ln r$, $A_k = -(r\,q\,\hat{J}'_\phi/s)_{r_k}$, and $B_k = -(r^2\,q\,\hat{J}''_\phi/s)_{r_k}$.

3. Neoclassical Physics

a. Plasma Species

The plasma is assumed to consist of three (charged) species; namely, electrons (e), majority ions (i), and impurity ions (I). The charges of the three species are $e_e = -e$, $e_i = e$, and $e_I = Z_I\,e$, respectively, where e is the magnitude of the electron charge. Quasi-neutrality demands that $n_e = n_i + Z_I\,n_I$, where $n_a(r)$ is the species-a number density. Let $\alpha_I(r) = Z_I\,(Z_{\rm eff} - 1)/(Z_I - Z_{\rm eff})$, where $Z_{\rm eff}(r) = (n_i + Z_I^2\,n_I)/n_e$ is the effective ion charge number. It follows that $n_i/n_e = (Z_I - Z_{\rm eff})/(Z_I - 1)$ and $n_I/n_e = (Z_{\rm eff} - 1)/[Z_I\,(Z_I - 1)]$. Finally, let $Z_{{\rm eff}\,i} = (Z_I - Z_{\rm eff})/(Z_I - 1)$, and $Z_{{\rm eff}\,I} = Z_I\,(Z_{\rm eff} - 1)/(Z_I - 1)$.

b. Collisionality Parameters

Consider an equilibrium magnetic flux-surface whose label is r. Let [23]

$$\frac{1}{\gamma(r)} = \frac{q}{g}\oint \frac{B\,R^2}{B_0\,R_0^2}\,\frac{d\theta}{2\pi}. \tag{A18}$$

It is helpful to define a new poloidal angle Θ such that

$$\frac{d\Theta}{d\theta} = \frac{\gamma\,q}{g}\,\frac{B\,R^2}{B_0\,R_0^2}. \tag{A19}$$

Let

$$I_1 = \oint \frac{B_0}{B}\,\frac{d\Theta}{2\pi}, \tag{A20}$$

$$I_2 = \oint \frac{B}{B_0}\,\frac{d\Theta}{2\pi}, \tag{A21}$$

$$I_3 = \oint \left(\frac{\partial B}{\partial \Theta}\right)^2 \frac{1}{B_0\,B}\,\frac{d\Theta}{2\pi}, \tag{A22}$$

$$I_{4,j} = \sqrt{2\,j}\oint \frac{\cos(j\,\Theta)}{B/B_0}\,\frac{d\Theta}{2\pi}, \tag{A23}$$

$$I_{5,j} = \sqrt{2\,j}\oint \frac{\cos(j\,\Theta)}{2\,(B/B_0)^{\,2}}\,\frac{d\Theta}{2\pi}, \tag{A24}$$

$$I_6(\lambda) = \oint \frac{\sqrt{1-\lambda\,B/B_{\rm max}}}{B/B_0}\,\frac{d\Theta}{2\pi}, \tag{A25}$$

where $B_{\rm max}$ is the maximum value of B on the magnetic flux-surface, and j a positive integer. The species-a transit frequency is written $\omega_{t\,a}(r) = K_t\,\gamma\,v_{T\,a}$, where

$$K_t(r) = \frac{I_1^{\,2}\,I_3}{I_2^{\,2}\,\sum_{j=1,\infty} I_{4,j}\,I_{5,j}}, \tag{A26}$$

and $v_{T\,a} = \sqrt{2\,T_a/m_a}$. Here, m_a is the species-a mass, and $T_a(r)$ the species-a temperature (in energy units). The fraction of circulating particles is

$$f_c(r) = \frac{3\,I_2}{4}\,\frac{B_0^{\,2}}{B_{\rm max}^{\,2}}\int_0^1 \frac{\lambda\,d\lambda}{I_6(\lambda)}. \tag{A27}$$

Finally, the dimensionless species-a collisionality parameter is written $\nu_{*\,a}(r) = K_*\,g_t/(\omega_{t\,a}\,\tau_{aa})$, where $g_t(r) = f_c/(1-f_c)$,

$$K_*(r) = \frac{3}{8\pi}\,\frac{I_2}{I_3}\,K_t^{\,2}, \tag{A28}$$

$$\frac{1}{\tau_{aa}(r)} = \frac{4}{3\sqrt{\pi}}\,\frac{4\pi\,n_a\,e_a^{\,4}\,\ln\Lambda}{(4\pi\,\epsilon_0)^{\,2}\,m_a^{\,2}\,v_{T\,a}^{\,3}}. \tag{A29}$$

Here, the Coulomb logarithm, $\ln\Lambda$, is assumed to take the same large constant value (i.e., $\ln\Lambda \simeq 17$), independent of species.

c. Collisional Friction Matrices

Let $x_{ab} = v_{T\,b}/v_{T\,a}$. The 2×2 dimensionless ion collisional friction matrices, $[F^{\,ii}](r)$, $[F^{\,iI}](r)$, $[F^{\,Ii}](r)$, and $[F^{\,II}](r)$, are defined to have the following elements:[23]

$$F_{00}^{\,ii} = \frac{\alpha_I\,(1+m_i/m_I)}{(1+x_{iI}^{\,2})^{\,3/2}}, \tag{A30}$$

$$F_{01}^{ii} = \frac{3}{2}\,\frac{\alpha_I\,(1+m_i/m_I)}{(1+x_{iI}^2)^{\,5/2}}, \tag{A31}$$

$$F_{11}^{ii} = \sqrt{2} + \frac{\alpha_I\,[13/4 + 4\,x_{iI}^2 + (15/2)\,x_{iI}^4]}{(1+x_{iI}^2)^{\,5/2}}, \tag{A32}$$

$$F_{01}^{iI} = \frac{3}{2}\,\frac{T_i}{T_I}\,\frac{\alpha_I\,(1+m_I/m_i)}{x_{iI}\,(1+x_{Ii}^2)^{\,5/2}}, \tag{A33}$$

$$F_{11}^{iI} = \frac{27}{4}\,\frac{T_i}{T_I}\,\frac{\alpha_I\,x_{iI}^2}{(1+x_{iI}^2)^{\,5/2}}, \tag{A34}$$

$$F_{11}^{Ii} = \frac{27}{4}\,\frac{\alpha_I\,x_{iI}^2}{(1+x_{iI}^2)^{\,5/2}}, \tag{A35}$$

$$F_{11}^{II} = \frac{T_i}{T_I}\left\{\sqrt{2}\,\alpha_I^2\,x_{Ii} + \frac{\alpha_I\,[15/2 + 4\,x_{iI}^2 + (13/4)\,x_{iI}^4]}{(1+x_{iI}^2)^{\,5/2}}\right\}, \tag{A36}$$

$F_{10}^{ii} = F_{01}^{ii}$, $F_{00}^{iI} = F_{00}^{ii}$, $F_{10}^{iI} = F_{01}^{ii}$, $F_{00}^{Ii} = F_{00}^{ii}$, $F_{01}^{Ii} = F_{01}^{ii}$, $F_{10}^{Ii} = F_{01}^{iI}$, $F_{00}^{II} = F_{00}^{ii}$, $F_{01}^{II} = F_{01}^{iI}$, $F_{10}^{II} = F_{01}^{iI}$.

The 2×2 dimensionless electron collisional friction matrices, $[F^{\,ee}](r)$, $[F^{\,ei}](r)$, and $[F^{\,eI}](r)$, are defined to have the following elements:[23] $F_{00}^{ee} = Z_{\rm eff}$, $F_{01}^{ee} = (3/2)\,Z_{\rm eff}$, $F_{10}^{ee} = F_{01}^{ee}$, $F_{11}^{ee} = \sqrt{2} + (13/4)\,Z_{\rm eff}$, $F_{00}^{ei} = Z_{{\rm eff}\,i}$, $F_{01}^{ei} = F_{11}^{ei} = 0$, $F_{10}^{ei} = (3/2)\,Z_{{\rm eff}\,i}$, $F_{00}^{eI} = Z_{{\rm eff}\,I}$, $F_{01}^{eI} = F_{11}^{eI} = 0$, $F_{10}^{eI} = (3/2)\,Z_{{\rm eff}\,I}$.

d. Neoclassical Viscosity Matrices

The 2×2 dimensionless species-a neoclassical viscosity matrix, $[\mu^{\,a}](r)$, is defined to have the following elements:[23] $\mu_{00}^a = K_{00}^a$, $\mu_{01}^a = (5/2)\,K_{00}^a - K_{01}^a$, $\mu_{10}^a = \mu_{01}^a$, $\mu_{11}^a = K_{11}^a - 5\,K_{01}^a + (25/4)\,K_{00}^a$. Here,

$$K_{jk}^e = g_t\,\frac{4}{3\sqrt{\pi}}\int_0^\infty \frac{e^{-x}\,x^{\,4+j+k}\,\nu_D^e(x)\,dx}{[x^{\,2} + \nu_{*\,e}\,\nu_D^e(x)]\,[x^{\,2} + (5\pi/8)\,(\omega_{t\,e}\,\tau_{ee})^{\,-1}\,\nu_T^e(x)]}, \tag{A37}$$

$$\nu_D^e = \frac{3\sqrt{\pi}}{4}\left[\left(1 - \frac{1}{2\,x}\right)\psi(x) + \psi'(x)\right] + \frac{3\sqrt{\pi}}{4}\,Z_{\rm eff}, \tag{A38}$$

$$\nu_\epsilon^e = \frac{3\sqrt{\pi}}{2}\,[\psi(x) - \psi'(x)]\,, \tag{A39}$$

$$\nu_T^a(x) = 3\,\nu_D^a(x) + \nu_\epsilon^a(x), \tag{A40}$$

and

$$\psi(x) = \frac{2}{\sqrt{\pi}}\int_0^x {\rm e}^{-t^{\,2}}\,dt - \frac{2}{\sqrt{\pi}}\,x\,{\rm e}^{-x^{\,2}}, \tag{A41}$$

$$\psi'(x) = \frac{2}{\sqrt{\pi}}\, x\, \mathrm{e}^{-x^2}. \tag{A42}$$

Furthermore,

$$K^i_{jk} = g_t\, \frac{4}{3\sqrt{\pi}} \int_0^\infty \frac{e^{-x}\, x^{2+j+k}\, \nu^i_D(x)\, dx}{[x + \nu_{*\,i}\, \nu^i_D(x)]\, [x + (5\pi/8)\, (\omega_{t\,i}\, \tau_{ii})^{-1}\, \nu^i_T(x)]}, \tag{A43}$$

$$\nu^i_D = \frac{3\sqrt{\pi}}{4} \left[\left(1 - \frac{1}{2\,x} \right) \psi(x) + \psi'(x) \right] \frac{1}{x} + \frac{3\sqrt{\pi}}{4}\, \alpha_I \left[\left(1 - \frac{x_{iI}}{2\,x} \right) \psi\left(\frac{x}{x_{iI}} \right) + \psi'\left(\frac{x}{x_{iI}} \right) \right] \frac{1}{x}, \tag{A44}$$

$$\nu^{\,i}_\epsilon = \frac{3\sqrt{\pi}}{2} \left[\psi(x) - \psi'(x) \right] \frac{1}{x} + \frac{3\sqrt{\pi}}{2}\, \alpha_I \left[\frac{m_i}{m_I}\, \psi\left(\frac{x}{x_{iI}} \right) - \psi'\left(\frac{x}{x_{iI}} \right) \right] \frac{1}{x}, \tag{A45}$$

and, finally,

$$K^I_{jk} = g_t\, \frac{4}{3\sqrt{\pi}} \int_0^\infty \frac{e^{-x}\, x^{2+j+k}\, \nu^I_D(x)\, dx}{[x + \nu_{*\,I}\, \nu^I_D(x)]\, [x + (5\pi/8)\, (\omega_{t\,I}\, \tau_{II})^{-1}\, \nu^I_T(x)]}, \tag{A46}$$

$$\nu^I_D = \frac{3\sqrt{\pi}}{4} \left[\left(1 - \frac{1}{2\,x} \right) \psi(x) + \psi'(x) \right] \frac{1}{x} + \frac{3\sqrt{\pi}}{4}\, \frac{1}{\alpha_I} \left[\left(1 - \frac{x_{Ii}}{2\,x} \right) \psi\left(\frac{x}{x_{Ii}} \right) + \psi'\left(\frac{x}{x_{Ii}} \right) \right] \frac{1}{x}, \tag{A47}$$

$$\nu^{\,I}_\epsilon = \frac{3\sqrt{\pi}}{2} \left[\psi(x) - \psi'(x) \right] \frac{1}{x} + \frac{3\sqrt{\pi}}{2}\, \frac{1}{\alpha_I} \left[\frac{m_I}{m_i}\, \psi\left(\frac{x}{x_{Ii}} \right) - \psi'\left(\frac{x}{x_{Ii}} \right) \right] \frac{1}{x}. \tag{A48}$$

e. Parallel Force and Heat Balance

Let $[\tilde{\mu}^{\,I}] = \alpha_I^2\, (T_i/T_I)\, x_{Ii}\, [\mu^{\,I}]$. The requirement of equilibrium force and heat balance parallel to the magnetic field leads us to define four 2×2 dimensionless ion matrices, $[L^{\,ii}](r)$, $[L^{\,iI}](r)$, $[L^{\,Ii}](r)$, and $[L^{\,II}](r)$, where [23]

$$\begin{pmatrix} [L^{\,ii}], & [L^{\,iI}] \\ [L^{\,Ii}], & [L^{\,II}] \end{pmatrix} = \begin{pmatrix} [F^{\,ii} + \mu^{\,i} + Y^{\,in}/y_n], & -[F^{\,iI}] \\ -[F^{\,Ii}], & [F^{\,II} + \tilde{\mu}^{\,I}] \end{pmatrix}^{-1} \begin{pmatrix} [F^{\,ii} + Y^{\,in}], & -[F^{\,iI}] \\ -[F^{\,Ii}], & [F^{\,II}] \end{pmatrix}, \tag{A49}$$

the additional four 2×2 dimensionless ion matrices, $[G^{ii}](r)$, $[G^{iI}](r)$, $[G^{Ii}](r)$, and $[G^{II}](r)$, where

$$\begin{pmatrix} [G^{ii}], & [G^{iI}] \\ [G^{Ii}], & [G^{II}] \end{pmatrix} = \tau_{ii}\,\langle\sigma\,v\rangle_i^{\rm cx}\,\langle n_n\rangle \begin{pmatrix} [F^{ii}+\mu^{i}+Y^{in}/y_n], & -[F^{iI}] \\ -[F^{Ii}], & [F^{II}+\tilde{\mu}^{I}] \end{pmatrix}^{-1}, \tag{A50}$$

and the 2×2 dimensionless electron matrices, $[Q^{ee}](r)$, $[G^{ei}](r)$, $[L^{ee}](r)$, $[L^{ei}](r)$, and $[L^{eI}](r)$, where

$$[Q^{ee}] = [F^{ee}+\mu^{e}]^{-1}, \tag{A51}$$

$$[G^{ei}] = [Q^{ee}]\,([F^{ei}]\,[G^{ii}] + [F^{eI}]\,[G^{Ii}]), \tag{A52}$$

$$[L^{ee}] = [Q^{ee}]\,[F^{ee}], \tag{A53}$$

$$[L^{ei}] = [Q^{ee}]\left\{[F^{ei}]\,[L^{ii}] - [F^{ei}] + [F^{eI}]\,[L^{Ii}]\right\}, \tag{A54}$$

$$[L^{eI}] = [Q^{ee}]\left\{[F^{eI}]\,[L^{II}] - [F^{eI}] + [F^{ei}]\,[L^{iI}]\right\}. \tag{A55}$$

Here,[30]

$$[Y^{in}] = \tau_{ii}\,\langle\sigma\,v\rangle_i^{\rm cx}\,\langle n_n\rangle \begin{bmatrix} 1, & 0 \\ 0, & E_n/T_i \end{bmatrix}, \tag{A56}$$

$$y_n = \frac{\langle n_n\rangle\,\langle B^2\rangle}{\langle n_n\,B^2\rangle}, \tag{A57}$$

where

$$\langle A\rangle(r) \equiv \oint \frac{A(r,\Theta)\,d\Theta}{B(r,\Theta)} \Big/ \oint \frac{d\Theta}{B(r,\Theta)}. \tag{A58}$$

Moreover, $\langle\sigma\,v\rangle_i^{\rm cx}$ is the flux-surface averaged rate constant for charge-exchange reactions between neutrals and majority ions, $n_n(r,\Theta)$ the neutral particle number density, and E_n/T_i the ratio of the incoming neutral energy to the majority ion energy. The parameter y_n takes into account the fact that the incoming neutrals at the edge of an H-mode tokamak plasma are usually concentrated at the X-point (i.e., $y_n > 1$).

f. Neoclassical Frequencies

The neoclassical frequencies of the three plasma species have the following definitions:

$$\omega_{{\rm nc}\,i}(r) = -G_{00}^{ii}\,\omega_E - \left[L_{00}^{ii} - L_{01}^{ii}\left(\frac{\eta_i}{1+\eta_i}\right)\right]\omega_{*\,i} - \left[L_{00}^{iI} - L_{01}^{iI}\left(\frac{\eta_I}{1+\eta_I}\right)\right]\omega_{*\,I}, \tag{A59}$$

$$\omega_{\mathrm{nc}\,I}(r) = -G_{00}^{Ii}\,\omega_E - \left[L_{00}^{II} - L_{01}^{II}\left(\frac{\eta_I}{1+\eta_I}\right)\right]\omega_{*\,I} - \left[L_{00}^{Ii} - L_{01}^{Ii}\left(\frac{\eta_i}{1+\eta_i}\right)\right]\omega_{*\,i}, \tag{A60}$$

$$\omega_{\mathrm{nc}\,e}(r) = -G_{00}^{ei}\,\omega_E - \left[L_{00}^{ee} - L_{01}^{ee}\left(\frac{\eta_e}{1+\eta_e}\right)\right]\omega_{*\,e} - \left[L_{00}^{ei} - L_{01}^{ei}\left(\frac{\eta_i}{1+\eta_i}\right)\right]\omega_{*\,i} - \left[L_{00}^{eI} - L_{01}^{eI}\left(\frac{\eta_I}{1+\eta_I}\right)\right]\omega_{*\,I}. \tag{A61}$$

Here,

$$\omega_E(r) = -\frac{d\Phi}{d\Psi_p}, \tag{A62}$$

$$\omega_{*\,a}(r) = -\frac{T_a}{e_a}\,\frac{d\ln p_a}{d\Psi_p}, \tag{A63}$$

$$\eta_a(r) = \frac{d\ln T_a}{d\ln n_a}. \tag{A64}$$

Moreover, $p_a(r) = n_a\,T_a$, and $\Phi(r)$ is the equilibrium electric scalar potential.

g. Impurity Ion Angular Rotation Velocities

Let

$$\omega_{\theta\,I}(r) = \frac{\mathbf{V}^{\,I}\cdot\nabla\theta}{\mathbf{B}\cdot\nabla\theta}\,\frac{R_0\,B_0\,g}{R^2}, \tag{A65}$$

$$\omega_{\phi\,I}(r) = \mathbf{V}^{\,I}\cdot\nabla\phi, \tag{A66}$$

where $\mathbf{V}^{\,I}$ is the impurity ion fluid velocity, and the right-hand sides are evaluated on the outboard mid-plane. According to neoclassical theory,[11]

$$\omega_{\theta\,I} = K_\theta\,\omega_{\mathrm{nc}\,I}, \tag{A67}$$

$$\omega_{\phi\,I} = \omega_E + \omega_{*\,I} + \omega_{\theta\,I}, \tag{A68}$$

where

$$K_\theta(r) = \frac{R_0^2\,B_0^2\,g^{\,2}}{R^2\,\langle B^{\,2}\rangle}. \tag{A69}$$

4. Plasma Response in Inner Region

a. Linear Layer Widths

Let

$$\tau_R(r) = \mu_0\,r^{\,2}\,\sigma_{ee}\,Q_{00}^{ee}, \tag{A70}$$

$$\sigma_{ee}(r) = \frac{n_e\, e^{\,2}\, \tau_{ee}}{m_e}, \tag{A71}$$

$$\tau_H(r) = \frac{R_0}{B_0\, g}\, \frac{\sqrt{\mu_0\, \rho}}{n\, s}, \tag{A72}$$

$$\rho(r) = m_i\, n_i(r) + m_I\, n_I(r), \tag{A73}$$

$$\tau_E(r) = \frac{r^{\,2}}{D_\perp + (2/3)\, \chi_e}, \tag{A74}$$

$$\tau_M(r) = \frac{R_0^2\, q^{\,2}}{\chi_\phi}, \tag{A75}$$

$$\rho_s(r) = \frac{\sqrt{m_i\, T_e}}{e\, B_0\, g}, \tag{A76}$$

$\tau(r) = -\omega_{*\,i}/\omega_{*\,e}$, $S(r) = \tau_R/\tau_H$, $P_M(r) = \tau_R/\tau_M$, $P_E(r) = \tau_R/\tau_E$, $D(r) = (5/3)\, S^{\,1/3}\, (\rho_s/r)$, $Q_E(r) = S^{\,1/3}\, n\, \omega_E\, \tau_H$, $Q_{e,i}(r) = -S^{\,1/3}\, n\, \omega_{*\,e,i}\, \tau_H$. Here, $\chi_e(r)$, $D_\perp(r)$, and $\chi_\phi(r)$ are the perpendicular electron energy, particle, and toroidal momentum diffusivity profiles, respectively. The constant-ψ linear layer width is determined from the solution of [31,32]

$$\frac{d^{\,2}\, Y}{dp^{\,2}} - \left[\frac{-Q_E\, (Q_E - Q_i) + \mathrm{i}\, (Q_E - Q_i)\, (P_M + P_E)\, p^{\,2} + P_M\, P_E\, p^{\,4}}{\mathrm{i}\, (Q_E - Q_e) + \{P_E + \mathrm{i}\, (Q_E - Q_i)\, D^{\,2}\}\, p^{\,2} + (1+\tau)\, P_M\, D^{\,2}\, p^{\,4}}\right] p^{\,2}\, Y = 0. \tag{A77}$$

If the small-p behavior of the solution of the previous equation that is well-behaved as $p \to \infty$ is $Y(p) = Y_0\, [1 - c\, p + \mathcal{O}(p^{\,2})]$ then the linear layer width is

$$\delta_{\rm linear}(r) = \frac{\pi\, |c|\, r}{S^{\,1/3}}. \tag{A78}$$

Note that Eq. (A77) can only be solved when $1 + \tau > 0$.

b. Island Widths

Let $\Psi_k = R_0\, B_0\, \hat{\Psi}_k\, \mathrm{e}^{-\mathrm{i}\,\varphi_k}$, where $\hat{\Psi}_k > 0$ and φ_k are both real quantities. The full width (in r) of the magnetic island chain at the kth resonant surface is [8]

$$W_k = 4\, R_0 \left(\frac{q}{g\, s}\right)_{r_k}^{1/2} \hat{\Psi}_k^{\,1/2}. \tag{A79}$$

c. Critical Island Widths

The critical full island width (in r) which must be exceeded before the electron temperature is flattened within the magnetic separatrix of the magnetic island chain at the kth

resonant surface is [7,33]

$$W_{T_e\,k} = 5.07 \left(\frac{\chi_e}{\chi_{\parallel\,e}}\right)_{r_k}^{1/4} \left(\frac{1}{\epsilon\, s\, n}\right)_{r_k}^{1/2} r_k, \tag{A80}$$

where $\epsilon = r/R_0$, and

$$\chi_{\parallel\,e} = \frac{\chi_{\parallel\,e}^{\rm brag}\,\chi_{\parallel\,e}^{\rm max}}{\chi_{\parallel\,e}^{\rm brag} + \chi_{\parallel\,e}^{\rm max}}, \tag{A81}$$

$$\chi_{\parallel\,e}^{\rm brag} = \frac{1.55\,\tau_{ee}\,v_{T\,e}^2}{1 + 0.38\,Z_{\rm eff}}, \tag{A82}$$

$$\chi_{\parallel\,e}^{\rm max} = \frac{2\,R_0\,v_{T\,e}}{n\,s}\,\frac{r_k}{W_{T_e\,k}} \tag{A83}$$

Equations (A80)–(A83) must be solved iteratively for $W_{T_e\,k}/r_k$.

The critical full island width (in r) which must be exceeded before the ion temperature is flattened within the magnetic separatrix of the magnetic island chain at the kth resonant surface is [7,33]

$$W_{T_i\,k} = 5.07 \left(\frac{\chi_i}{\chi_{\parallel\,i}}\right)_{r_k}^{1/4} \left(\frac{1}{\epsilon\, s\, n}\right)_{r_k}^{1/2} r_k, \tag{A84}$$

where $\chi_i(r)$ is the perpendicular ion energy diffusivity profile,

$$\chi_{\parallel\,i} = \frac{\chi_{\parallel\,i}^{\rm brag}\,\chi_{\parallel\,i}^{\rm max}}{\chi_{\parallel\,i}^{\rm brag} + \chi_{\parallel\,i}^{\rm max}}, \tag{A85}$$

$$\chi_{\parallel\,i}^{\rm brag} = 1.95\,\tau_{ii}\,v_{T\,i}^2, \tag{A86}$$

$$\chi_{\parallel\,i}^{\rm max} = \frac{2\,R_0\,v_{T\,i}}{n\,s}\,\frac{r_k}{W_{T_i\,k}}. \tag{A87}$$

Equations (A84)–(A87) must be solved iteratively for $W_{T_i\,k}/r_k$.

The critical full island width (in r) which must be exceeded before the electron density is flattened within the magnetic separatrix of the magnetic island chain at the kth resonant surface is [7,33]

$$W_{n_e\,k} = 5.07 \left(\frac{D_\perp}{\chi_{\parallel\,i}}\right)_{r_k}^{1/4} \left(\frac{1}{\epsilon\, s\, n}\right)_{r_k}^{1/2} r_k, \tag{A88}$$

where

$$\chi_{\parallel\,i} = \frac{\chi_{\parallel\,i}^{\rm brag}\,\chi_{\parallel\,i}^{\rm max}}{\chi_{\parallel\,i}^{\rm brag} + \chi_{\parallel\,i}^{\rm max}}, \tag{A89}$$

$$\chi_{\parallel\,i}^{\rm brag} = 1.95\,\tau_{ii}\,v_{T\,i}^2, \tag{A90}$$

$$\chi_{\parallel\,i}^{\rm max} = \frac{2\,R_0\,v_{T\,i}}{n\,s}\,\frac{r_k}{W_{n_e\,k}}. \tag{A91}$$

Equations (A88)–(A91) must be solved iteratively for $W_{n_e\,k}/r_k$.

d. Resonant Plasma Response Model

Let $\chi_k = R_0\, B_0\, \hat{\chi}_k\, \mathrm{e}^{-\mathrm{i}\,\zeta_k}$, and $E_{kk'} = \hat{E}_{kk'}\, \mathrm{e}^{-\mathrm{i}\,\xi_{kk'}}$, where $\hat{\chi}_k > 0$, ζ_k, $\hat{E}'_{kk} > 0$, and $\xi_{kk'}$ are all real quantities. Furthermore, let $X_k = \hat{\Psi}_k \cos\varphi_k$ and $Y_k = \hat{\Psi}_k \sin\varphi_k$. The resonant plasma response model at the kth resonant surface takes the form [8,10]

$$\left(\hat{W}_k + \hat{\delta}_k\right) \mathcal{S}_k \left(\frac{dX_k}{d\hat{t}} + \hat{\varpi}_k\, Y_k\right) = f_k\, X_k + \sum_{k'=1,K} \hat{E}_{kk'} \left(\cos\xi_{kk'}\, X_{k'} - \sin\xi_{kk'}\, Y_{k'}\right) + \hat{E}_{kk}\, \hat{\chi}_k\, \cos\zeta_k, \tag{A92}$$

$$\left(\hat{W}_k + \hat{\delta}_k\right) \mathcal{S}_k \left(\frac{dY_k}{d\hat{t}} - \hat{\varpi}_k\, X_k\right) = f_k\, Y_k + \sum_{k'=1,K} \hat{E}_{kk'} \left(\cos\xi_{kk'}\, Y_{k'} + \sin\xi_{kk'}\, X_{k'}\right) + \hat{E}_{kk}\, \hat{\chi}_k\, \sin\zeta_k, \tag{A93}$$

where

$$\hat{W}_k = \frac{\mathcal{I}\, W_k}{2\, r_k} = \frac{2\,\mathcal{I}}{\epsilon_{100}\, \hat{r}_k} \left(\frac{q}{g\, s}\right)_{r_k}^{1/2} \left(X_k^2 + Y_k^2\right)^{1/4}, \tag{A94}$$

$$\hat{\delta}_k = \frac{\delta_{\mathrm{linear}}(r_k)}{R_0\, \epsilon_{100}\, \hat{r}_k}, \tag{A95}$$

$$\mathcal{S}_k = \frac{\tau_R(r_k)}{\tau_A}, \tag{A96}$$

$$\tau_A = \left[\frac{\mu_0\, \rho(0)\, r_{100}^2}{B_0^2}\right]^{1/2}, \tag{A97}$$

$$f_k = f_{b\,k} + f_{c\,k} + f_{p\,k} + f_{s\,k}. \tag{A98}$$

Here, $\mathcal{I} = 0.8227$, $\epsilon_{100} = r_{100}/R_0$, $\hat{r} = r/r_{100}$, $\hat{r}_k = r_k/r_{100}$, and $\hat{t} = t/\tau_A$.

The perturbed bootstrap current terms in the resonant response model take the form [34,35]

$$f_{b\,k} = f_{b\,e\,k} + f_{b\,i\,k}, \tag{A99}$$

$$f_{b\,e\,k} = \alpha_{b\,e\,k} \left(f_{b\,T_e\,k} + f_{b\,n_e\,k}\right), \tag{A100}$$

$$f_{b\,i\,k} = \alpha_{b\,i\,k} \left(f_{b\,T_i\,k} + f_{b\,n_i\,k}\right), \tag{A101}$$

$$f_{b\,T_e\,k} = \left(\frac{\eta_e}{1+\eta_e}\right)_{r_k} \frac{\hat{W}_k}{\hat{W}_{T_e\,k}^2 + \hat{\rho}_{\theta\,e\,k}^2 + \hat{W}_k^2}, \tag{A102}$$

$$f_{b\,n_e\,k} = \left(\frac{1}{1+\eta_e}\right)_{r_k} \frac{\hat{W}_k}{\hat{W}_{n_e\,k}^2 + \hat{\rho}_{\theta\,e\,k}^2 + \hat{W}_k^2}, \tag{A103}$$

$$f_{b\,T_i\,k} = \left(\frac{\eta_i}{1+\eta_i}\right)_{r_k} \frac{\hat{W}_k}{\hat{W}_{T_i\,k}^2 + \hat{\rho}_{\theta\,i\,k}^2 + \hat{W}_k^2}, \tag{A104}$$

$$f_{b\,n_i\,k} = \left(\frac{1}{1+\eta_i}\right)_{r_k} \frac{\hat{W}_k}{\hat{W}_{n_e\,k}^2 + \hat{\rho}_{\theta\,i\,k}^2 + \hat{W}_k^2}, \tag{A105}$$

where

$$\alpha_{b\,e\,k} = -2\,\mathcal{I}\,I_g \left(\frac{\omega_{*\,e} + \omega_{\mathrm{nc}\,e}}{\omega_\beta}\right)_{r_k}, \tag{A106}$$

$$\alpha_{b\,i\,k} = 2\,\mathcal{I}\,I_g \left[\frac{(n_i/n_e)\,(\omega_{*\,i} + \omega_{\mathrm{nc}\,i}) + (Z_I\,n_I/n_e)\,(\omega_{*\,I} + \omega_{\mathrm{nc}\,I})}{\omega_\beta}\right]_{r_k}, \tag{A107}$$

$$\omega_\beta(r) = \frac{s\,g\,B_0}{\mu_0\,n_e\,e\,R_0^2\,q}, \tag{A108}$$

$$\hat{W}_{T_e\,k} = \frac{\mathcal{I}\,W_{T_e\,k}}{2\,r_k}, \tag{A109}$$

$$\hat{W}_{T_i\,k} = \frac{\mathcal{I}\,W_{T_i\,k}}{2\,r_k}, \tag{A110}$$

$$\hat{W}_{n_e\,k} = \frac{\mathcal{I}\,W_{n_e\,k}}{2\,r_k}, \tag{A111}$$

$$\hat{\rho}_{\theta\,e\,k} = \left(\frac{\mathcal{I}\,\rho_{\theta\,e}}{2\,r}\right)_{r_k} = \left(\frac{2\,\mathcal{I}\,v_{T\,e}\,m_e\,q\,R_0}{e\,B_0\,g\,r^{\,2}}\right)_{r_k}, \tag{A112}$$

$$\hat{\rho}_{\theta\,i\,k} = \left(\frac{\mathcal{I}\,\rho_{\theta\,i}}{2\,r}\right)_{r_k} = \left(\frac{2\,\mathcal{I}\,v_{T\,i}\,m_i\,q\,R_0}{e\,B_0\,g\,r^{\,2}}\right)_{r_k}, \tag{A113}$$

and $I_g = 1.58$.

The magnetic field-line curvature terms in the resonant response model take the form [34,35]

$$f_{c\,k} = \alpha_{c\,k}\,(f_{c\,T_e\,k} + f_{c\,n_e\,k} + f_{c\,T_i\,k} + f_{c\,n_i\,k}), \tag{A114}$$

$$f_{c\,T_e\,k} = \left(\frac{n_e}{n_e+n_i}\,\frac{\eta_e}{1+\eta_e}\right)_{r_k} \frac{\hat{W}_k}{\hat{W}_{T_e\,k}^2 + \hat{W}_k^2}, \tag{A115}$$

$$f_{c\,n_e\,k} = \left(\frac{n_e}{n_e+n_i}\,\frac{1}{1+\eta_e}\right)_{r_k} \frac{\hat{W}_k}{\hat{W}_{n_e\,k}^2 + \hat{W}_k^2}, \tag{A116}$$

$$f_{c\,T_i\,k} = \left(\frac{n_i}{n_e+n_i}\,\frac{\eta_i}{1+\eta_i}\right)_{r_k} \frac{\hat{W}_k}{\hat{W}_{T_i\,k}^2 + \hat{W}_k^2}, \tag{A117}$$

$$f_{c\,n_i\,k} = \left(\frac{n_i}{n_e+n_i}\,\frac{1}{1+\eta_i}\right)_{r_k} \frac{\hat{W}_k}{\hat{W}_{n_e\,k}^2 + \hat{W}_k^2}, \tag{A118}$$

where

$$\alpha_{c\,k} = 2\,\mathcal{I}\,I_g\,D_R(r_k). \tag{A119}$$

Here, $D_R(r)$ is the Glasser-Greene-Johnson resistive interchange stability parameter. (See Sect. A 2 e.)

The ion polarization terms in the resonant response model take the form [34,35]

$$f_{p\,k} = \alpha_{p\,k}\,(f_{p\,T_i\,k} + f_{p\,n_i\,k})\,, \tag{A120}$$

$$f_{p\,T_i\,k} = \left(\frac{\eta_i}{1+\eta_i}\right)_{r_k} \frac{\hat{W}_k}{(\hat{W}_{T_i\,k}^2 + \hat{W}_k^2)^{\,2}}, \tag{A121}$$

$$f_{p\,n_i\,k} = \left(\frac{1}{1+\eta_i}\right)_{r_k} \frac{\hat{W}_k}{(\hat{W}_{n_e\,k}^2 + \hat{W}_k^2)^{\,2}}, \tag{A122}$$

where

$$\alpha_{p\,k} = 8\,\mathcal{I}^3\,I_p \left[\frac{(\omega_{*\,i} + \omega_{\mathrm{nc}\,i})\,\omega_{\mathrm{nc}\,i}}{\omega_\beta\,\omega_\Omega}\right]_{r_k}, \tag{A123}$$

$$\omega_\Omega(r) = \frac{e\,g\,B_0\,s\,q}{m_i} \tag{A124}$$

and $I_p = 1.38$.

Finally, the island saturation terms in the resonant response model take the form [36]

$$f_{s\,k} = -(0.8\,A_k^2 - 0.27\,B_k - 0.09\,A_k)\,\frac{W_k}{r_k}. \tag{A125}$$

5. Plasma Angular Velocity Evolution

a. Evolution Equations

The quantity $\hat{\varpi}_k$ that appears in Eqs. (A92) and (A93) evolves in time according to [8]

$$\hat{\varpi}_k(\hat{t}) = \hat{\varpi}_{k\,0} - \sum_{k'=1,K}^{p=1,\infty} \frac{m_k}{m_{k'}}\,\frac{y_p(\hat{r}_k)}{y_p(\hat{r}_{k'})}\,\alpha_{k',p}(\hat{t}) - \sum_{k'=1,K}^{p=1,\infty} \frac{z_p(\hat{r}_k)}{z_p(\hat{r}_{k'})}\,\beta_{k',p}(\hat{t}), \tag{A126}$$

Here, $\hat{\varpi}_{k\,0} = \varpi_{k\,0}\,\tau_A$, $y_p(\hat{r}) = J_1(j_{1,p}\,\hat{r})/\hat{r}$, and $z_p(\hat{r}) = J_0(j_{0,p}\,\hat{r})$. Moreover, $\varpi_{k\,0}$ is the so-called "natural frequency" (in the absence of the RMP) at the kth resonant surface; this quantity is defined as the helical phase velocity of a naturally unstable island chain, resonant at the surface, in the absence of an RMP (or any other island chains). Furthermore, $J_m(z)$ is a standard Bessel function, and $j_{m,p}$ denotes the pth zero of this function. The time evolution equations for the $\alpha_{k,p}$ and $\beta_{k,p}$ parameters specify how the plasma poloidal and toroidal angular velocity profiles are modified by the electromagnetic torques that develop

within the plasma, in response to the applied RMP, and how these modifications affect the natural frequencies. The evolution equations take the form [8]

$$(1+2\,Q_k^2)\,\frac{d\alpha_{k,p}}{d\hat{t}}+\left(\frac{j_{1,p}^2}{\hat{\tau}_{M\,k}}+\frac{1}{\hat{\tau}_{\theta\,k}}+\frac{1}{\hat{\tau}_{\rm cx\,k}}\right)\alpha_{k,p}=\frac{m_k^2\,[y_p(\hat{r}_k)]^{\,2}}{\hat{\rho}_k\,\epsilon_{100}^2\,[J_2(j_{1,p})]^{\,2}}\,\delta\hat{T}_k, \tag{A127}$$

$$\frac{d\beta_{k,p}}{d\hat{t}}+\left(\frac{j_{0,p}^2}{\hat{\tau}_{M\,k}}+\frac{1}{\hat{\tau}_{\rm cx\,k}}\right)\beta_{k,p}=\frac{n^{\,2}\,[z_p(\hat{r}_k)]^{\,2}}{\hat{\rho}_k\,[J_1(j_{0,p})]^{\,2}}\,\delta\hat{T}_k, \tag{A128}$$

where

$$\delta\hat{T}_k=\sum_{k'=1,K}\hat{E}_{kk'}\,[(Y_k\,X_{k'}-X_k\,Y_{k'})\,\cos\xi_{kk'}-(X_k\,X_{k'}+Y_k\,Y_{k'})\,\sin\xi_{kk'}]$$

$$+\,\hat{E}_{kk}\,\hat{\chi}_k\,(Y_k\,\cos\zeta_k-X_k\,\sin\zeta_k). \tag{A129}$$

Here, $Q_k=Q(r_k)$, $\hat{\rho}_k=\rho(r_k)/\rho(0)$, $\hat{\tau}_{M\,k}=r_{100}^2/[\chi_\phi(r_k)\,\tau_A]$, $\hat{\tau}_{\theta\,k}=\tau_\theta(r_k)/\tau_A$, $\hat{\tau}_{\rm cx\,k}=\tau_{\rm cx}(r_k)/\tau_A$. Moreover,

$$\tau_\theta(r)=\frac{\tau_{ii}}{\mu_{00}^i}\bigg/\left(1+\frac{q^{\,2}\,R_0^2}{r^{\,2}\,a_{kk}}\right). \tag{A130}$$

is the poloidal flow damping timescale, and

$$\tau_{\rm cx}(r)=\frac{1}{\langle n_n\rangle\,\langle\sigma\,v\rangle_i^{\rm cx}} \tag{A131}$$

is the charge-exchange damping timescale. Furthermore,[37]

$$Q^{\,2}(r)=\frac{q^{\,2}\,R_0^2}{2\,r^{\,2}}\left(\left\langle\frac{1}{R^2}\right\rangle-\frac{1}{\langle R^2\rangle}\right)\bigg/\left\langle\frac{|\nabla r|^{\,2}}{R^2}\right\rangle. \tag{A132}$$

b. Natural Frequencies

According to linear tearing mode theory, in the absence of the RMP, the natural frequency of the tearing mode resonant at the kth resonant surface is given by [8,31]

$$\varpi_{e\,k}=-n\,(\omega_E+\omega_{*\,e})_{r_k}. \tag{A133}$$

According to nonlinear tearing mode theory, in the absence of the RMP, the natural frequency of the tearing mode resonant at the kth resonant surface is given by [8,34,35]

$$\varpi_{i\,k}=-n\,(\omega_E+\omega_{*\,i}+\omega_{{\rm nc}\,i})_{r_k}. \tag{A134}$$

It is also helpful to define

$$\varpi_{E\,k}=-n\,(\omega_E)_{r_k}. \tag{A135}$$

The EPEC model for the natural frequency is

$$\varpi_{k\,0} = \varpi_{E\,k} + (\varpi_{e\,k} - \varpi_{E\,k})\, f_{e\,k} + (\varpi_{i\,k} - \varpi_{E\,k})\, f_{i\,k}, \tag{A136}$$

where

$$f_{e\,k} = f_{T_e\,k} + f_{n_e\,k}, \tag{A137}$$

$$f_{i\,k} = f_{T_i\,k} + f_{n_i\,k}, \tag{A138}$$

$$f_{T_e\,k} = \left(\frac{\eta_e}{1+\eta_e}\right)_{r_k} \frac{\hat{W}^2_{T_e\,k}}{\hat{W}^2_{T_e\,k} + \hat{W}^2_k}, \tag{A139}$$

$$f_{n_e\,k} = \left(\frac{1}{1+\eta_e}\right)_{r_k} \frac{\hat{W}^2_{n_e\,k}}{\hat{W}^2_{n_e\,k} + \hat{W}^2_k}, \tag{A140}$$

$$f_{T_i\,k} = \left(\frac{\eta_i}{1+\eta_i}\right)_{r_k} \frac{\hat{W}^2_k}{\hat{W}^2_{T_i\,k} + \hat{W}^2_k}, \tag{A141}$$

$$f_{n_i\,k} = \left(\frac{1}{1+\eta_i}\right)_{r_k} \frac{\hat{W}^2_k}{\hat{W}^2_{n_e\,k} + \hat{W}^2_k}. \tag{A142}$$

Note that the switch-over from linear to nonlinear theory is triggered by the flattening of the local temperature and density profiles.

DATA AVAILABILITY STATEMENT

The data that support the findings of this study are available from the corresponding author upon reasonable request.

REFERENCES

[1] J.A. Wesson, *Tokamaks*, 4th Edition. Oxford University Press (2011).

[2] R.J. Buttery, S. Günter, G. Giruzzi, T.C. Hender, D. Howell, G. Huysmans, R.J. La Haye, M. Maraschek, H. Reimerdes, O. Sauter, C.D. Warrick, H.R. Wilson, and H. Zohm, Plasma Phys. Control. Fusion **42**, B61 (2000).

[3] R.J. La Haye, Phys. Plasmas **13**, 055501 (2006).

[4] Z. Chang, J.D. Callen, E.D. Fredrickson, R.V. Budny, C.C. Hegna, K.M. McGuire, M.C. Zarnstorff, and TFTR group, Phys. Rev. Lett. **74**, 4663 (1995).

[5] R.J. Bickerton, J.W. Connor, and J.B. Taylor, Nat. Phys. Sci. **229** (1971).

[6] R. Carrera, R.D. Hazeltine, and M. Kotschenreuther, Phys. Fluids **29**, 899 (1986).

[7] R. Fitzpatrick, Phys. Plasmas **2**, 825 (1995).

[8] R. Fitzpatrick, and A.O. Nelson, Phys. Plasmas **27**, 072501 (2020).

[9] R. Fitzpatrick, Phys. Plasmas **27**, 102511 (2020).

[10] R. Fitzpatrick, Phys. Plasmas **28**, 022503 (2021).

[11] R. Fitzpatrick, S.-K. Kim, and J. Lee, Phys. Plasmas **28**, 082511 (2021).

[12] H.P. Furth, J. Killeen, and M.N. Rosenbluth, Phys. Fluids **6**, 459 (1963).

[13] B. Coppi, J.M. Greene, and J.L. Johnson, Nucl. Fusion **6**, 101 (1966).

[14] P.H. Rutherford, Phys. Fluids **16**, 1903 (1973).

[15] G. Ara, B. Basu, B. Coppi, G. Laval, M.N. Rosenbluth, and B.V. Waddell, Ann. Phys. (N.Y.) **112**, 443 (1978).

[16] A. Pletzer, and R.L. Dewar, J. Plasma Physics **45**, 427 (1991).

[17] R. Fitzpatrick, Nucl. Fusion **33**, 1049 (1993).

[18] R. Fitzpatrick, R.J. Hastie, T.J. Martin, and C.M. Roach, Nucl. Fusion **33**, 1533 (1993).

[19] S. Tokuda, Nucl. Fusion **41**, 1037 (2001).

[20] D.P. Brennan, R.J. La Haye, A.D. Turnbull, M.S. Chu, T.H. Jensen, L.L. Lao, T.C. Luce, P.A. Politzer, and E.J. Strait, Phys. Plasmas **10**, 1643 (2003).

[21] A.H. Glasser, Z.R. Wang, and J.-K. Park, Phys. Plasmas **23**, 112506 (2016).

[22] R. Fitzpatrick, Phys. Plasmas **24**, 072506 (2017).

[23] S.P. Hirshman, and D.J. Sigmar, Nucl. Fusion **21**, 1079 (1981).

[24] J.M. Canik, R. Maingi, T.E. Evans, R.E. Bell, S.P. Gerhardt, H.W. Kugel, B.P. LeBlanc, J. Manickam, J.E. Menard, T.H. Osborne, J.-K. Park, S. Paul, P.B. Snyder, S.A. Sabbagh, E.A. Unterberg, and the NSTX team, Nucl. Fusion **50**, 034012 (2010).

[25] C.F. Barnett, *Atomic Data for Fusion* (Oak Ridge National Laboratory, TN, 1990). Vol. 1, p. ORNL-6086.

[26] S.J. Zweben, J.R. Myra, A. Diallo, D.A. Russell, F. Scotti, and D.P. Stotler, Phys. Plasmas **26**, 072502 (2019).

[27] O. Meneghini, S.P. Smith, L.L. Lao, O. Izacard, Q. Ren, J.M. Park, J. Candy, *et al.*, Nucl. Fusion **55**, 083008 (2015).

[28] J.-K. Park, and N.C. Logan, Phys. Plasmas **24**, 032505 (2017).

[29] A.H. Glasser, J.M. Greene, and J.L. Johnson, Phys. Fluids **18**, 875 (1975).

[30] P. Monier-Garbet, K.H. Burrell, F.L. Hinton, J. Kim, X. Garbet, and R.J. Groebner, Nucl. Fusion **37**, 403 (1997).

[31] A. Cole and R. Fitzpatrick, Phys. Plasmas **13**, 032503 (2006).

[32] R. Fitzpatrick, Phys. Plasmas **29**, 032507 (2022).

[33] S.I. Braginskii. In *Reviews of Plasma Physics*. Vol. I, 205. Consultants Bureau (New York, NY, 1965).

[34] R. Fitzpatrick, Phys. Plasmas **23**,052506 (2016).

[35] R. Fitzpatrick, Phys. Plasmas **25**, 082513 (2018).

[36] R.J. Hastie, F. Militello, and F. Porcelli, Phys. Rev. Lett. **95**, 065001 (2005).

[37] S.P. Hirshman, Nucl. Fusion **18**, 7 (1978).

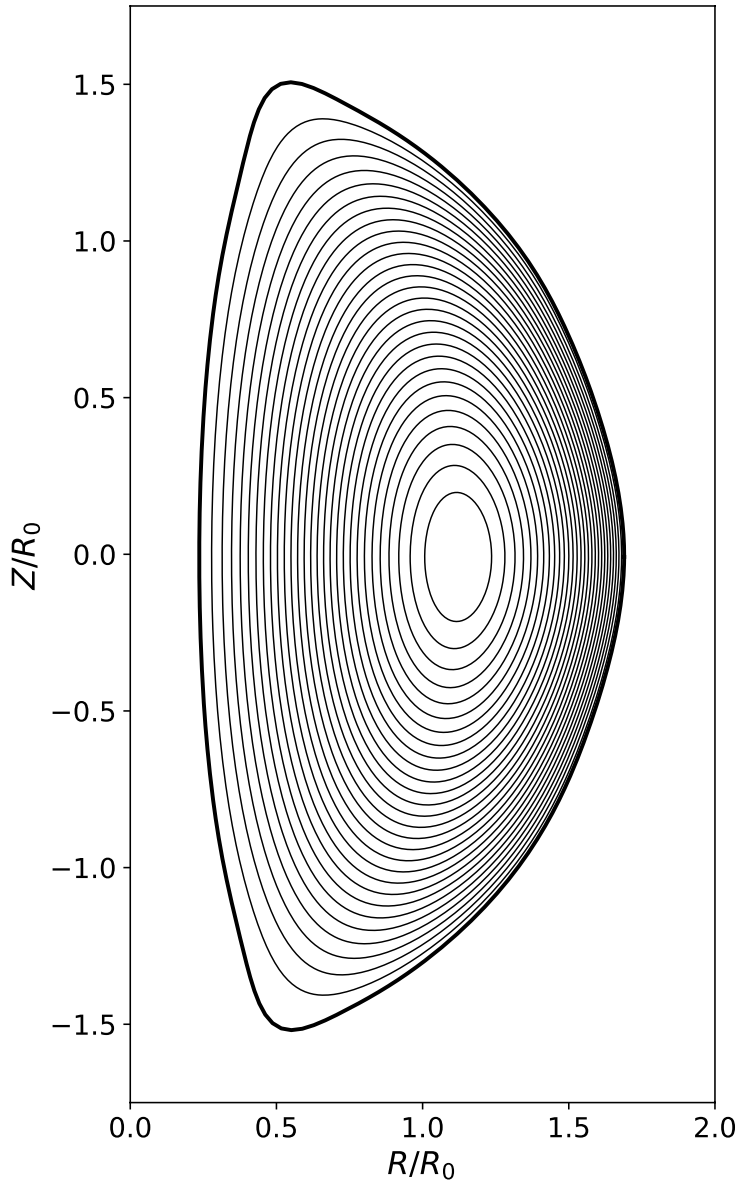

FIG. 1. Equilibrium magnetic flux-surfaces in NSTX discharge 127317 at $t = 400$ ms. Here, $R_0 = 0.85$ m.

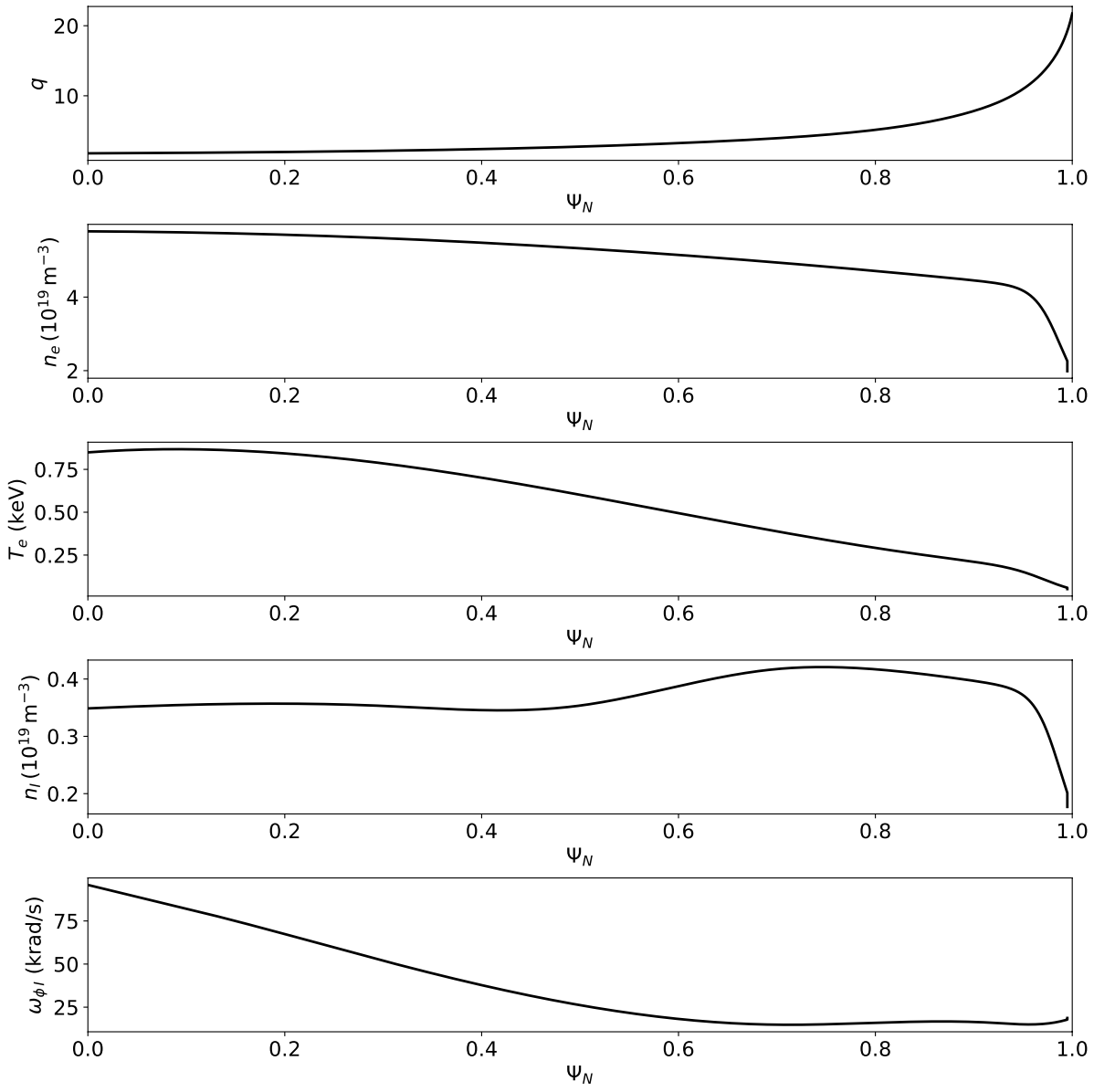

FIG. 2. The safety-factor, electron number density, electron temperature, impurity ion number density, and impurity ion toroidal rotation profiles in NSTX discharge 127317 at $t = 400$ ms.

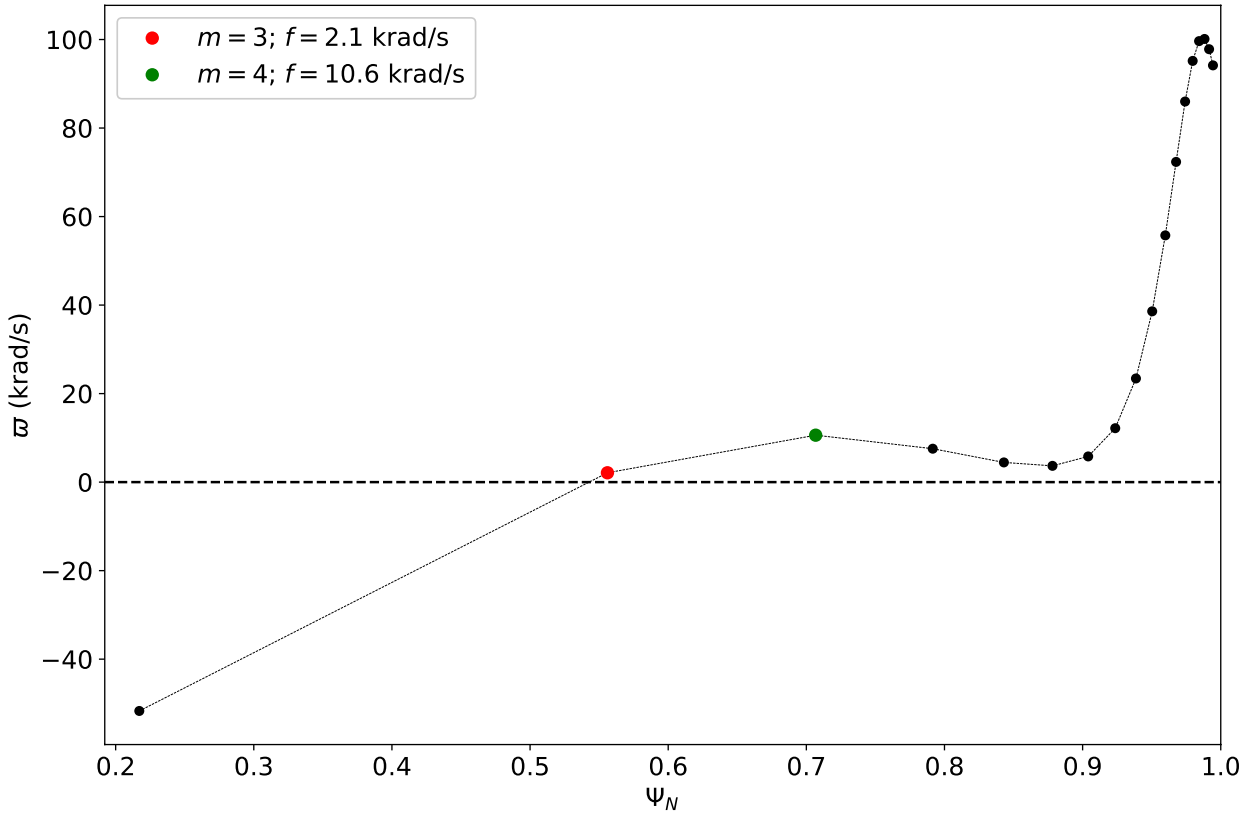

FIG. 3. Linear $n = 1$ natural frequencies in NSTX discharge 127317 at $t = 400$ ms. There are 18 $n = 1$ resonant surfaces in the plasma corresponding to $m = 2$ through $m = 19$. Only the $m = 3$ and $m = 4$ surfaces are potentially unstable to NTMs.

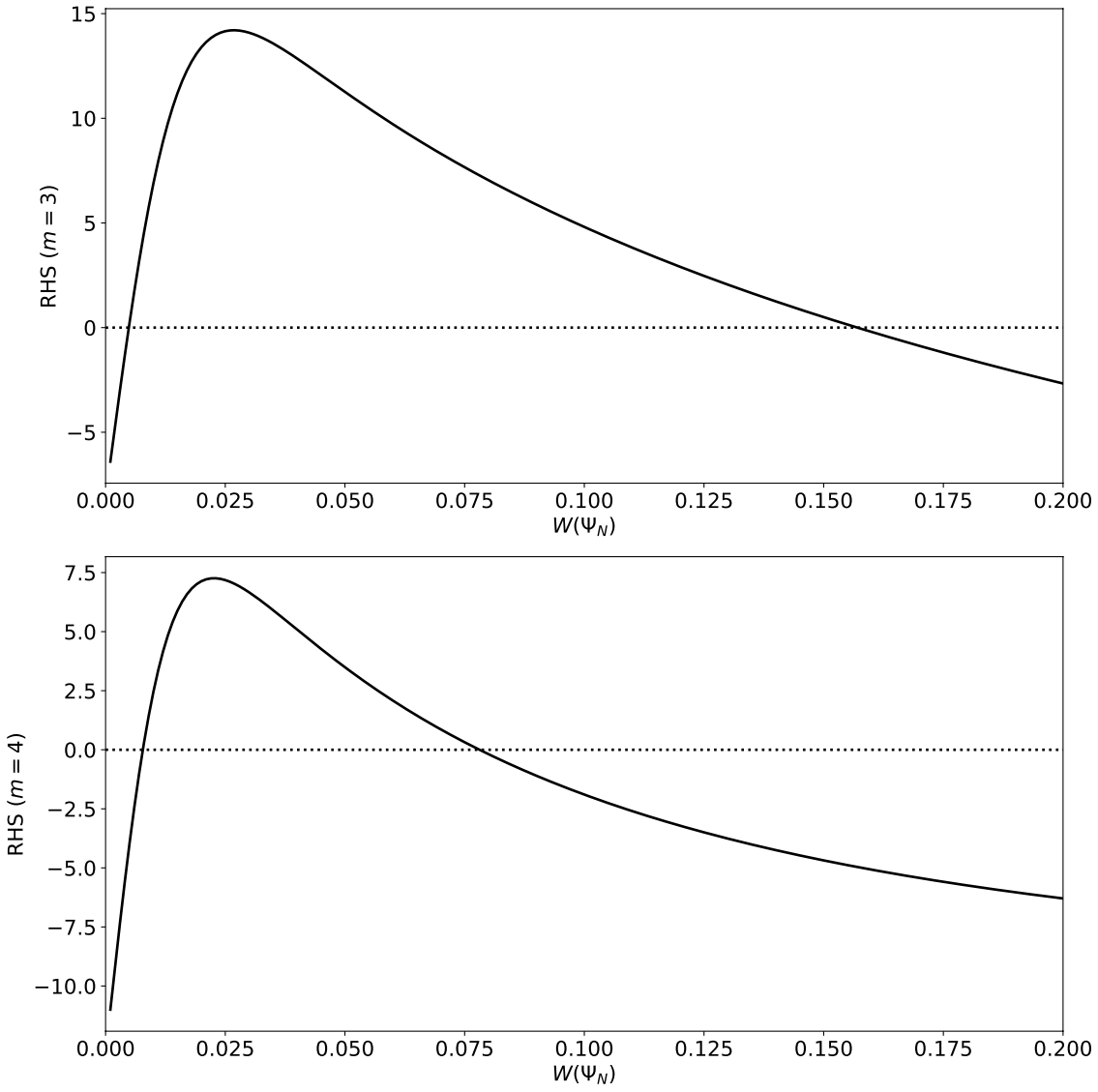

FIG. 4. Right-hand sides of modified Rutherford equations for $m = 3/n = 1$ and $m = 4/n = 1$ tearing modes in NSTX discharge 127317 at $t = 400$ ms.

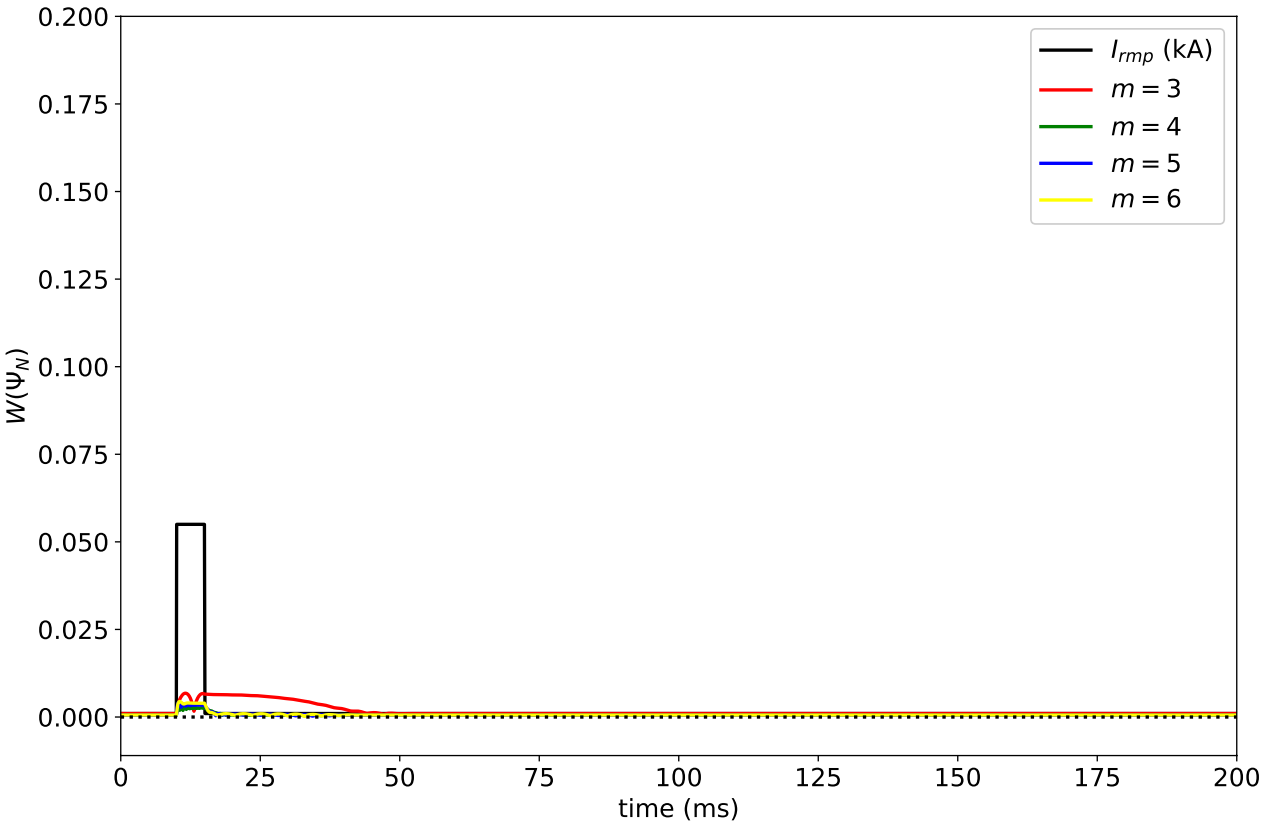

FIG. 5. Calculated $n = 1$ island widths versus time in NSTX discharge 127317 in response to an $n = 1$ current pulse of amplitude 0.055 kA, duration 5 ms, and frequency 0 krad/s applied to the RMP coils.

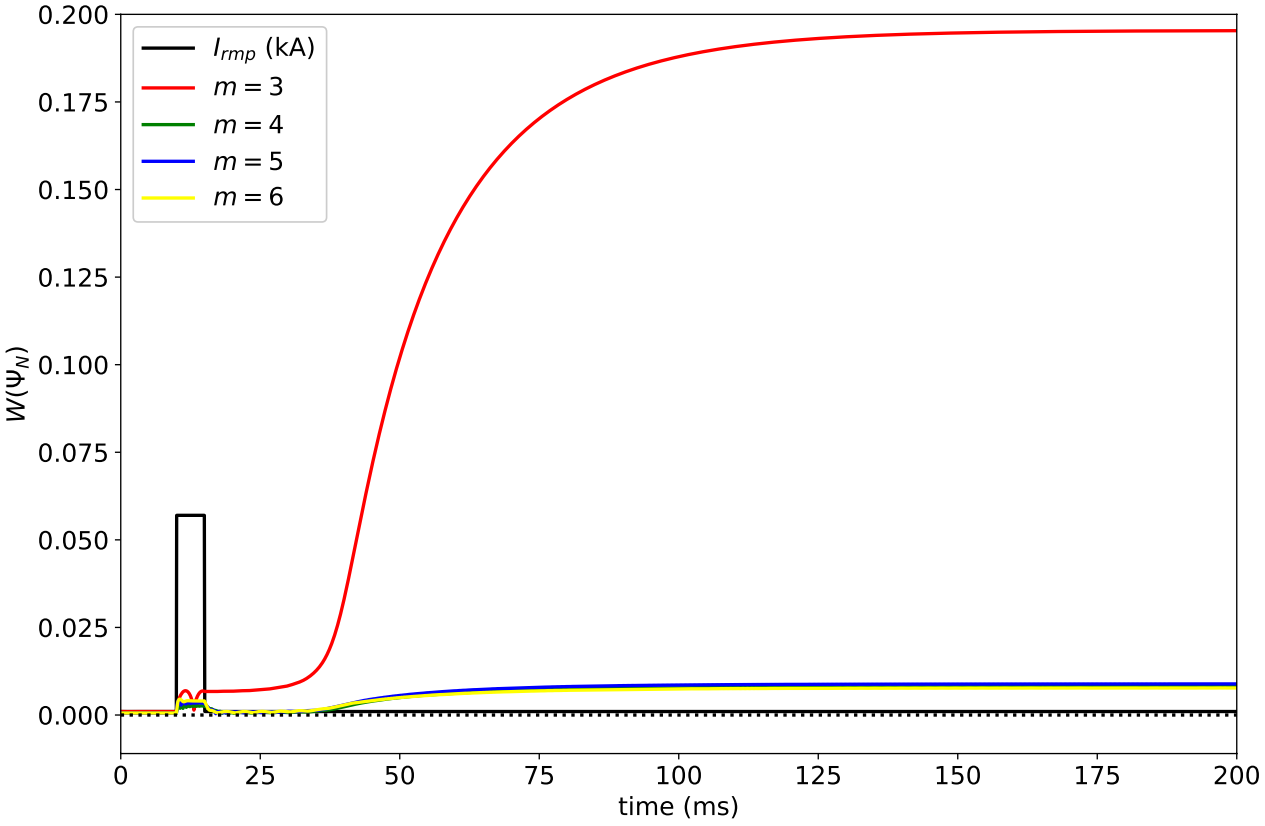

FIG. 6. Calculated $n = 1$ island widths versus time in NSTX discharge 127317 in response to an $n = 1$ current pulse of amplitude 0.057 kA, duration 5 ms, and frequency 0 krad/s applied to the RMP coils.

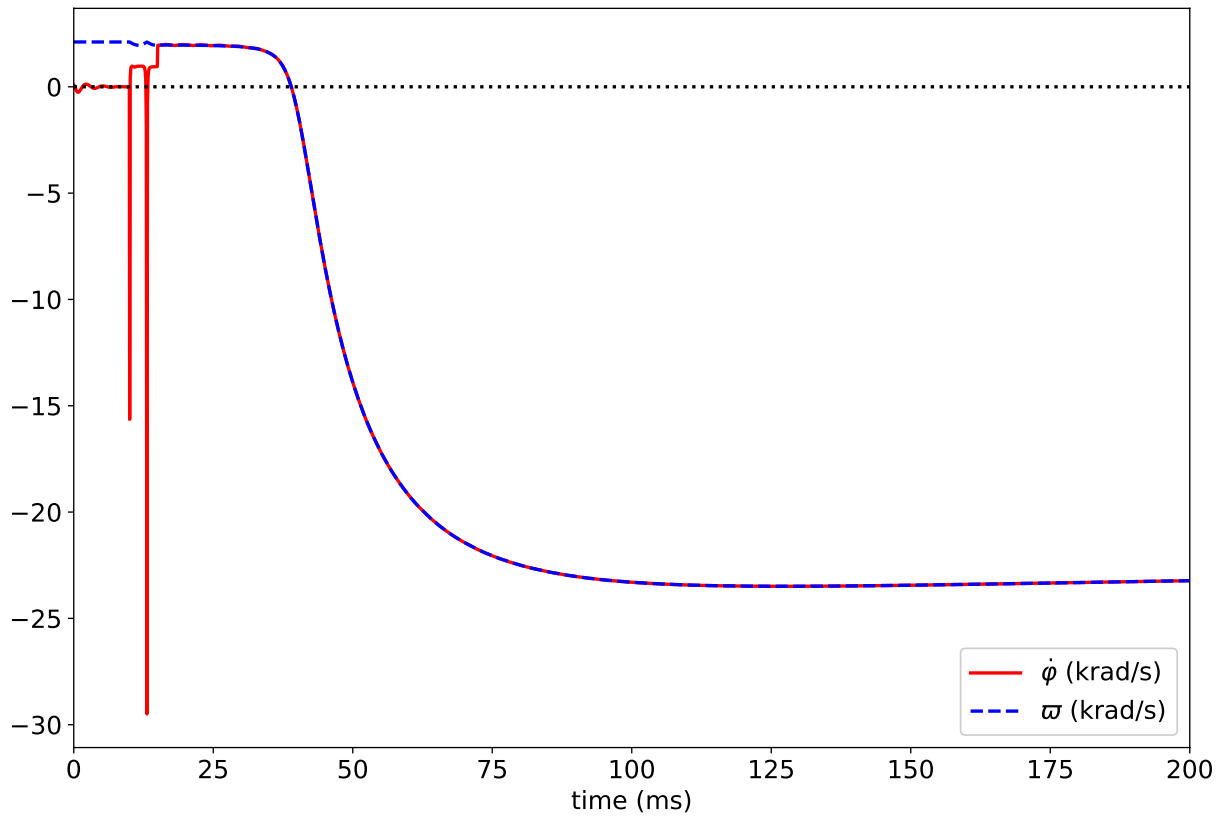

FIG. 7. Calculated phase velocity ($\dot{\varphi}$) and natural frequency (ϖ) of $m = 3/n = 1$ mode versus time in NSTX discharge 127317 in response to an $n = 1$ current pulse of amplitude 0.057 kA, duration 5 ms, and frequency 0 krad/s applied to the RMP coils.

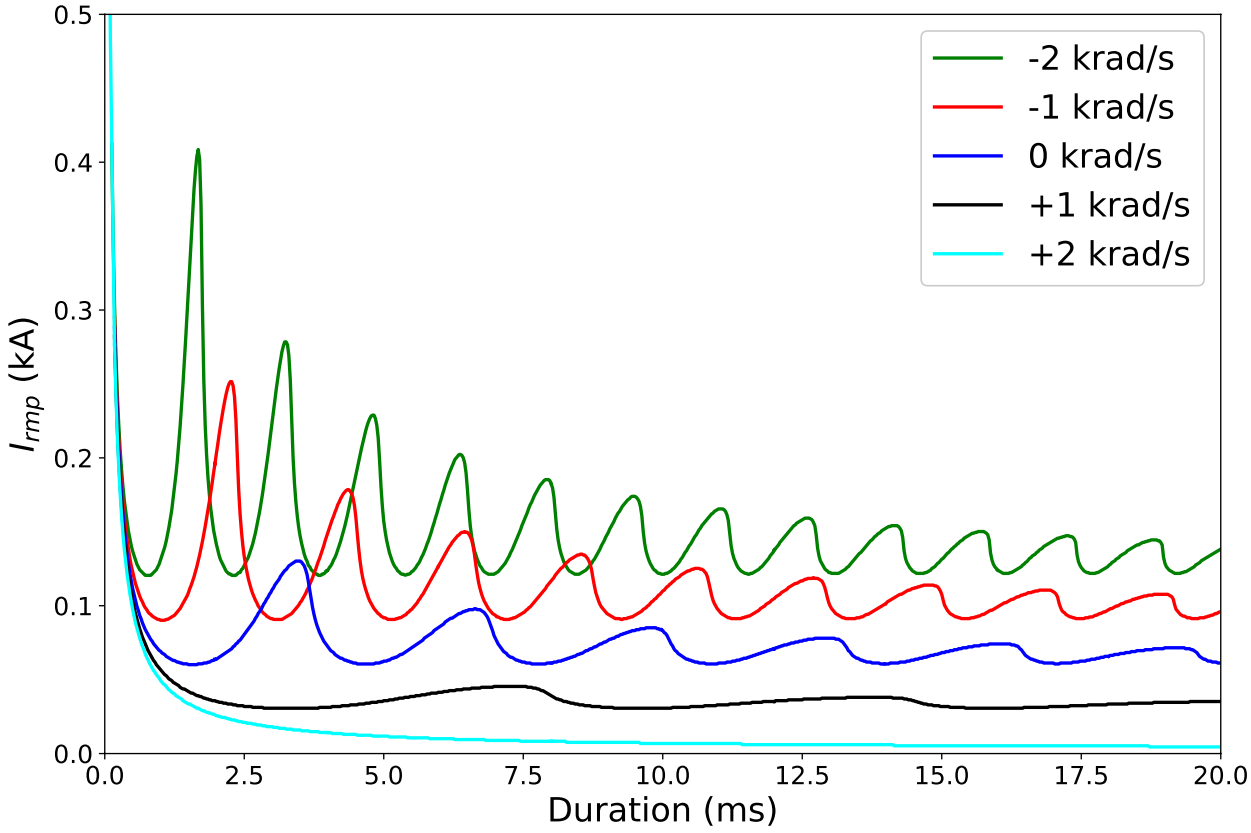

FIG. 8. Critical $n = 1$ RMP coil current pulse amplitude required to trigger an $m = 3/n = 1$ NTM in NSTX discharge 127317 as a function of the pulse duration for various different pulse frequencies.

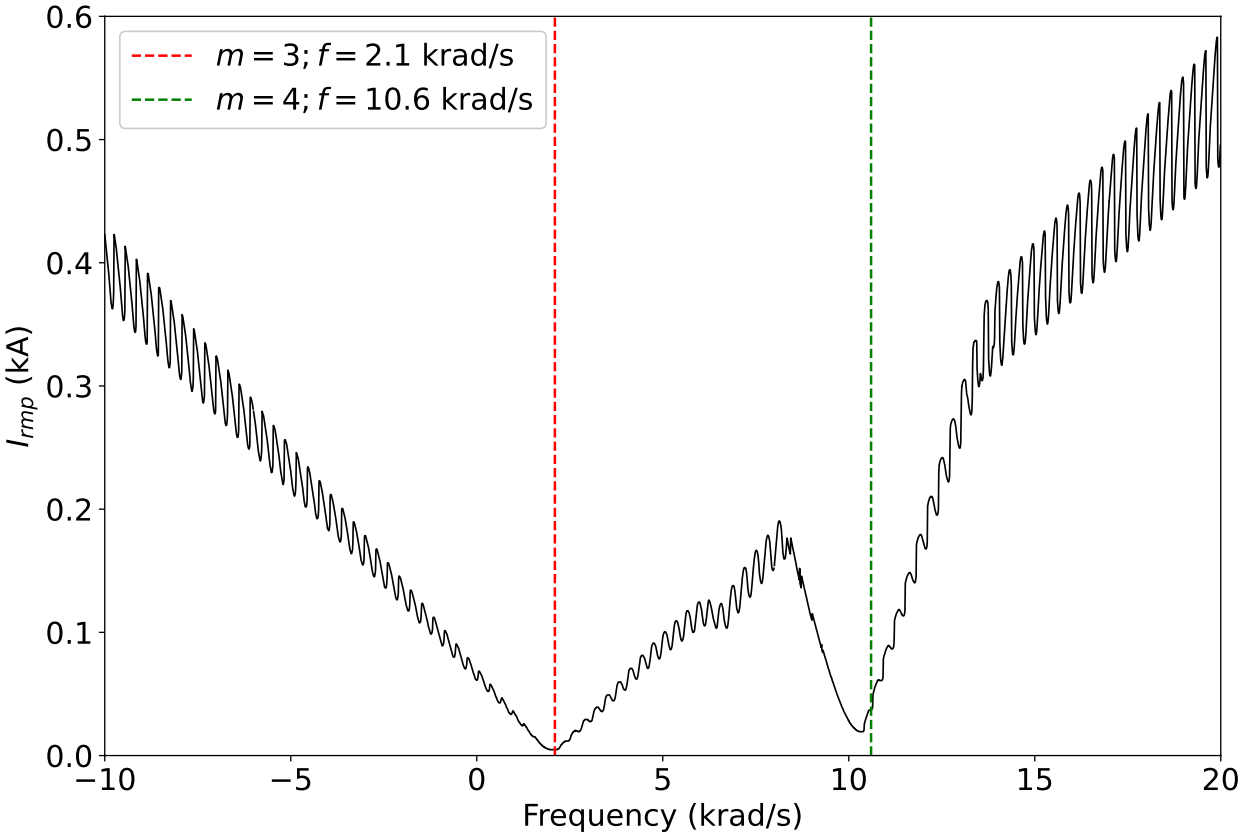

FIG. 9. Critical $n = 1$ RMP coil current pulse amplitude required to trigger an $m = 3/n = 1$ NTM in NSTX discharge 127317 as a function of the pulse frequency for a pulse duration of 20 ms.

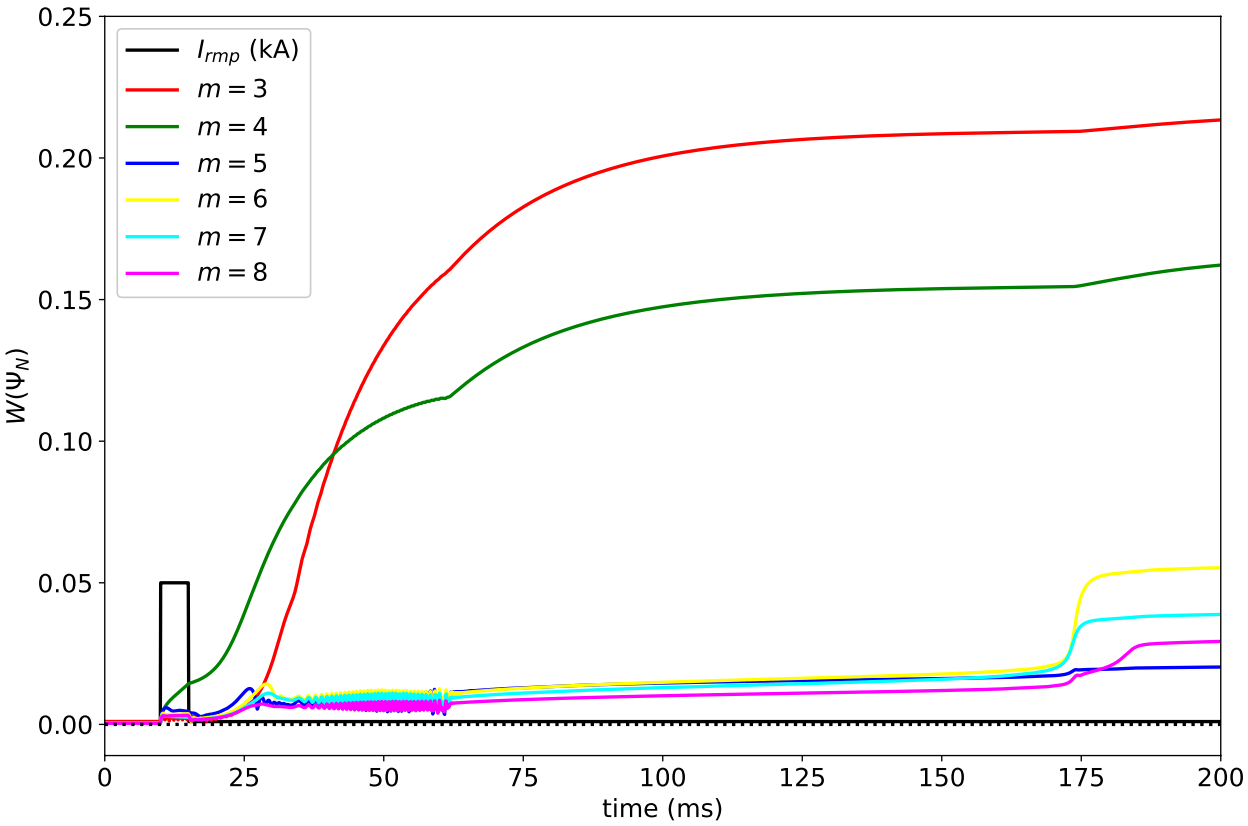

FIG. 10. Calculated $n = 1$ island widths versus time in NSTX discharge 127317 in response to an $n = 1$ current pulse of amplitude 0.05 kA, duration 5 ms, and frequency 10 krad/s applied to the RMP coils.

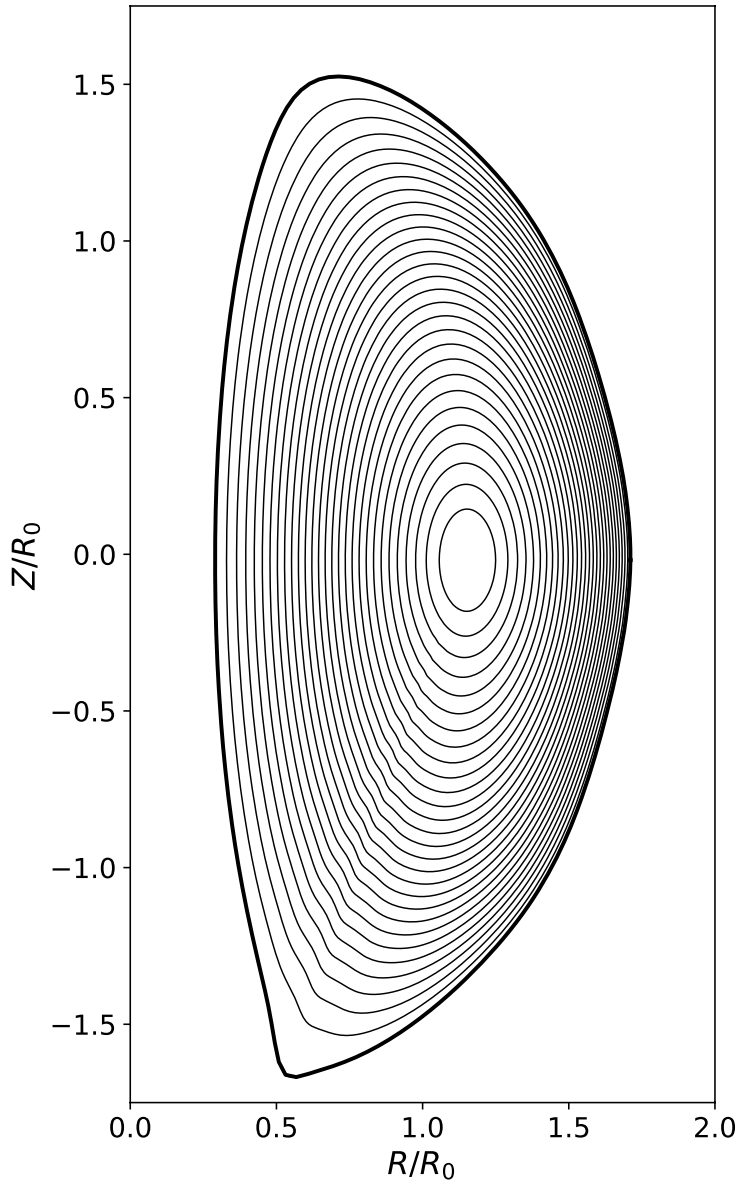

FIG. 11. Equilibrium magnetic flux-surfaces in NSTX discharge 139057 at $t = 557$ ms. Here, $R_0 = 0.85$ m.

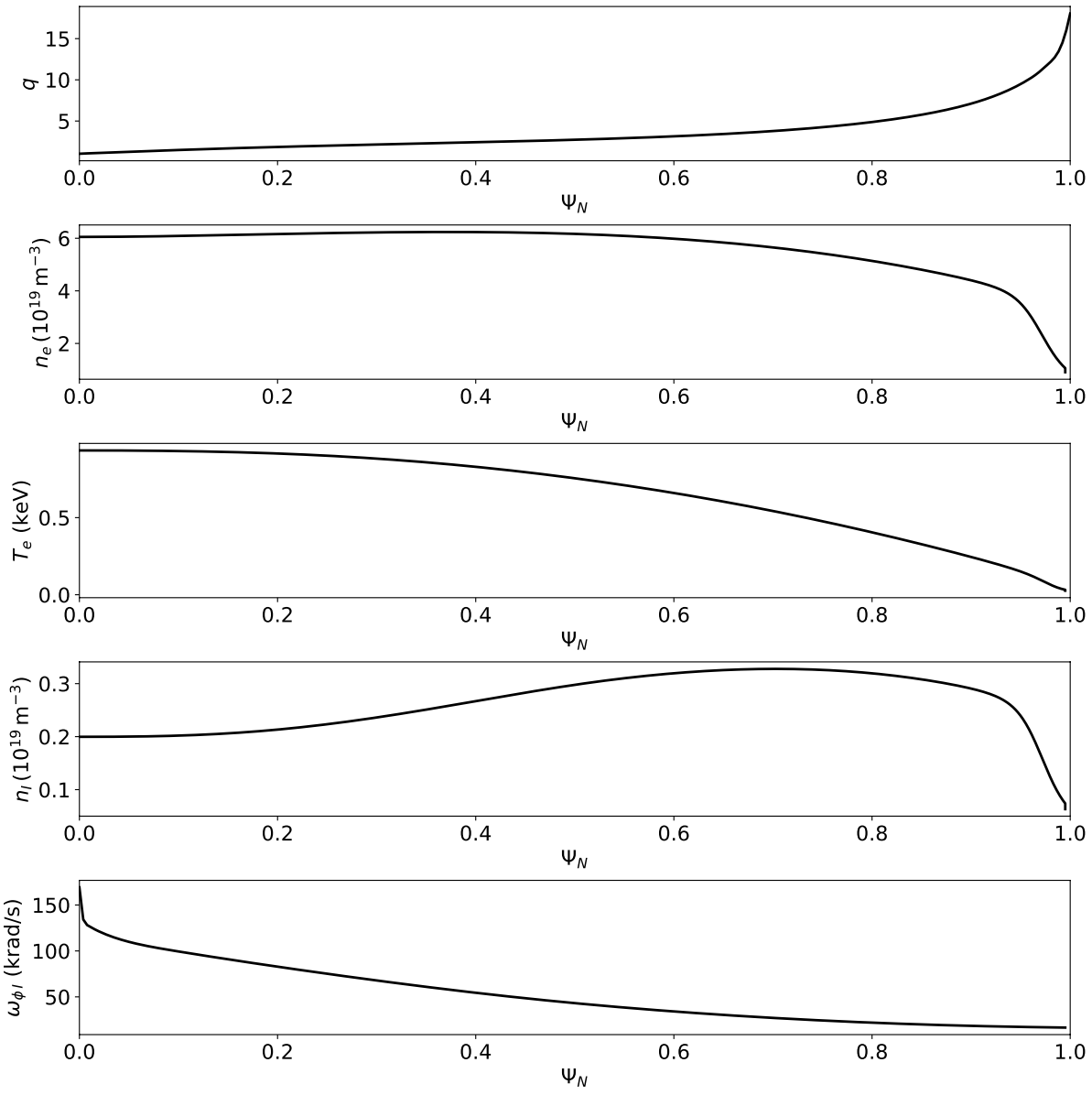

FIG. 12. The safety-factor, electron number density, electron temperature, impurity ion number density, and impurity ion toroidal rotation profiles in NSTX discharge 139057 at $t = 557$ ms.

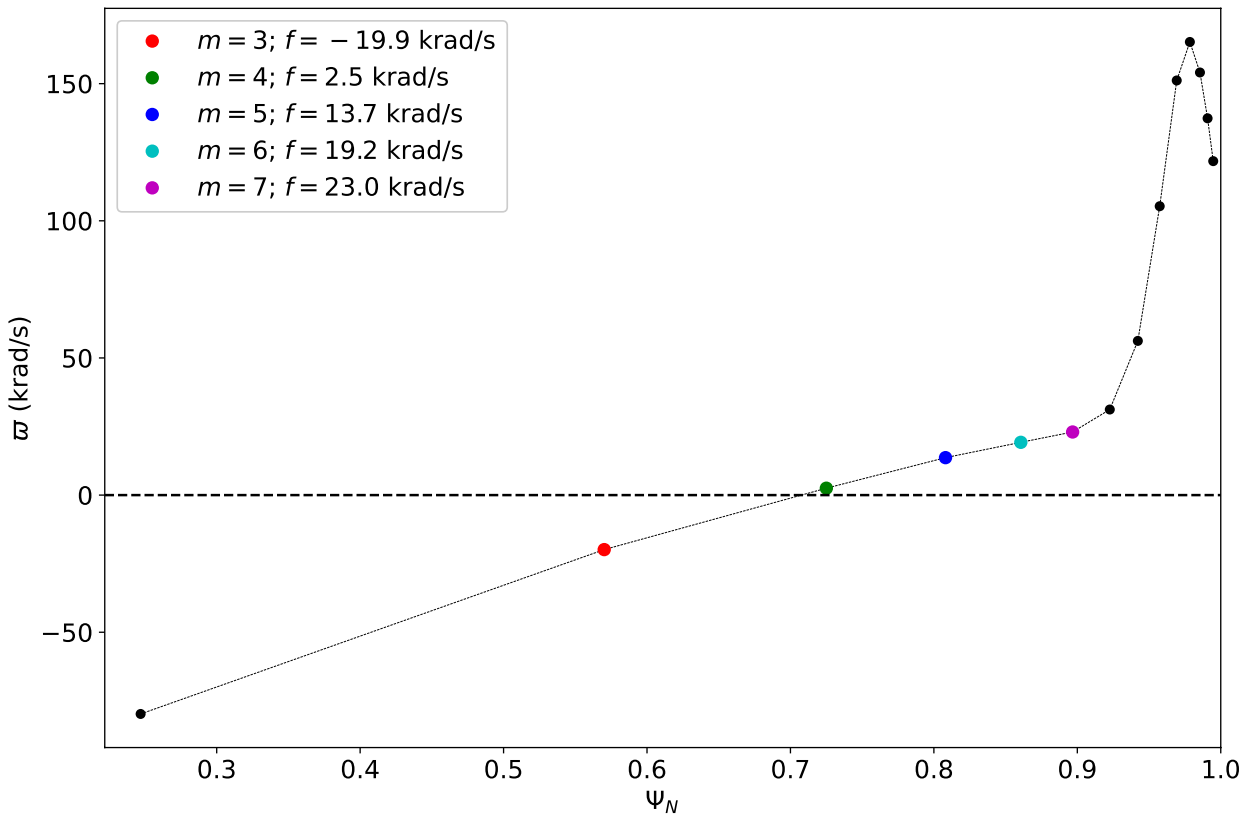

FIG. 13. Linear $n = 1$ natural frequencies in NSTX discharge 139057 at $t = 557$ ms. There are 14 $n = 1$ resonant surfaces in the plasma corresponding to $m = 2$ through $m = 15$. Only the $m = 3$, 4, 5, 6, and 7 surfaces are potentially unstable to NTMs.

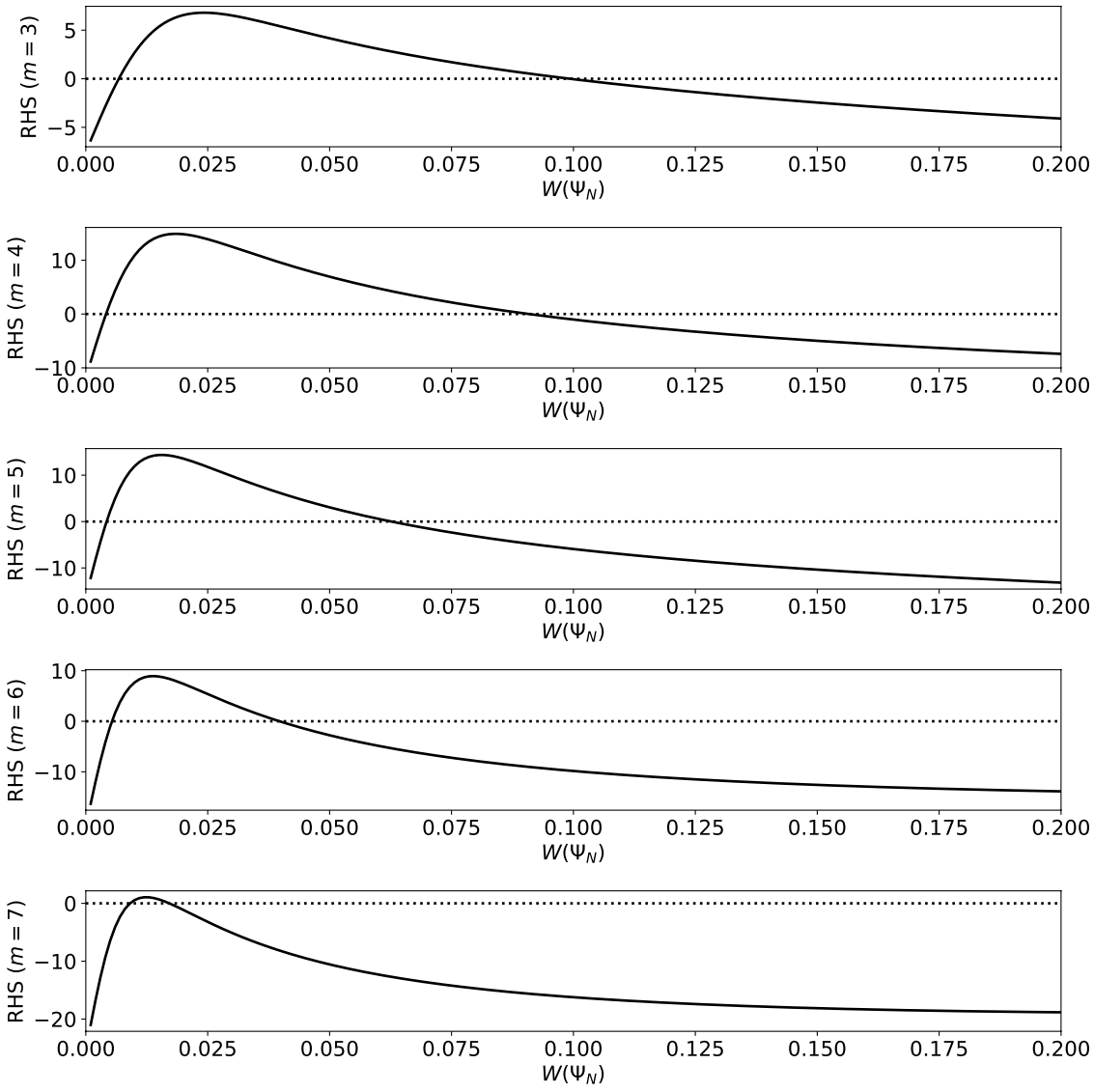

FIG. 14. Right-hand sides of modified Rutherford equations for $m = 3/n = 1$, 4/1, 5/1, 6/1, and 7/1 tearing modes in NSTX discharge 139057 at $t = 557$ ms.

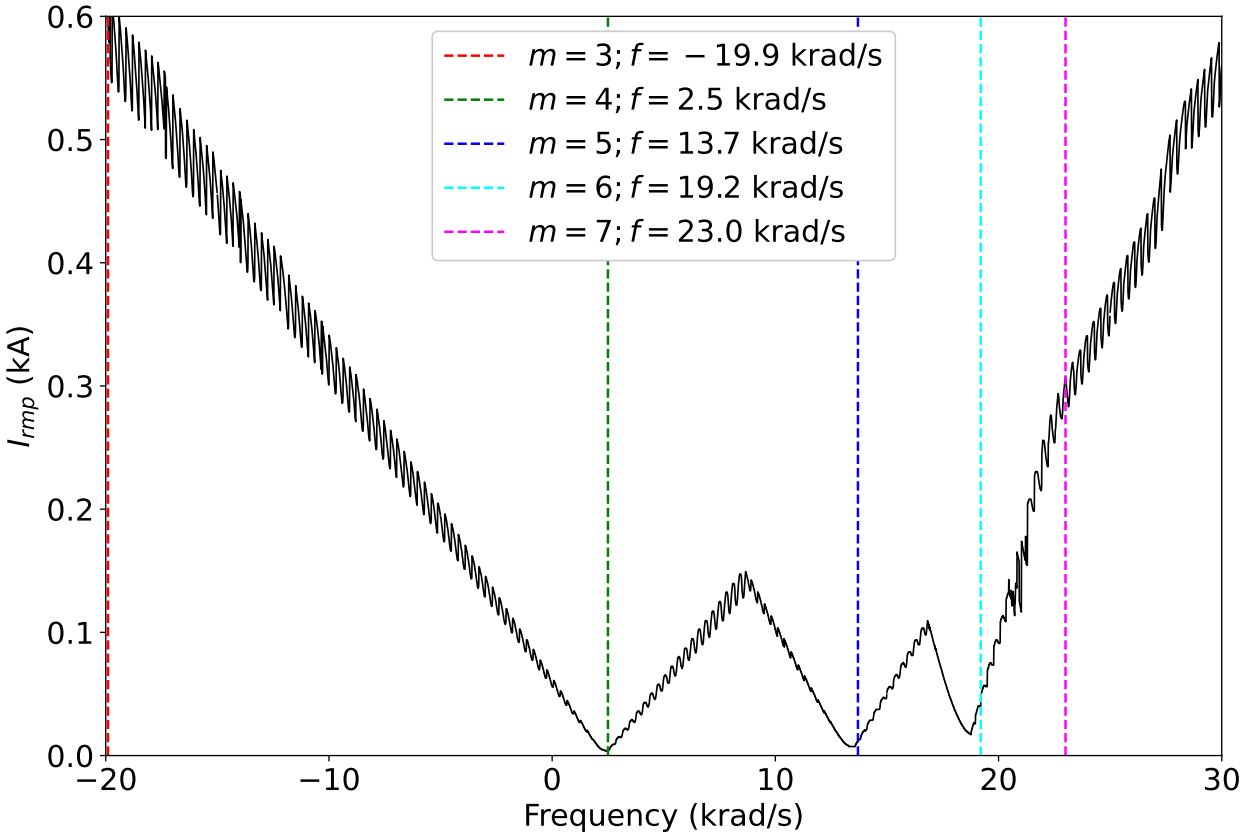

FIG. 15. Critical $n = 1$ RMP coil current pulse amplitude required to trigger an $m = 4/n = 1$ NTM in NSTX discharge 139057 as a function of the pulse frequency for a pulse duration of 20 ms.